

Scalable Design with Posterior-Based Operating Characteristics

Luke Hagar* Nathaniel T. Stevens

*Department of Statistics & Actuarial Science
University of Waterloo, Waterloo, ON, Canada, N2L 3G1*

Abstract

To design trustworthy Bayesian studies, criteria for posterior-based operating characteristics – such as power and the type I error rate – are often defined in clinical, industrial, and corporate settings. These posterior-based operating characteristics are typically assessed by exploring sampling distributions of posterior probabilities via simulation. In this paper, we propose a scalable method to determine optimal sample sizes and decision criteria that maps posterior probabilities to low-dimensional conduits for the data. Our method leverages this mapping and large-sample theory to explore sampling distributions of posterior probabilities in a targeted manner. This targeted exploration approach prompts consistent sample size recommendations with fewer simulation repetitions than standard methods. We repurpose the posterior probabilities computed in that approach to efficiently investigate various sample sizes and decision criteria using contour plots.

Keywords: Design priors; experimental design; interval hypotheses; low-discrepancy sequences; the Bernstein-von Mises theorem

1 Introduction

In recent decades, Bayesian methods for data-driven decision making have become increasingly popular. Two-group comparisons have long been a cornerstone of statistical analysis. Posterior analyses that compare scalar quantities θ_1 and θ_2 are often of interest, where the characteristic θ_j describes a comparison ($j = 1$) or reference ($j = 2$) group. This paper emphasizes two-group comparisons facilitated via the posterior of $\theta = \theta_1 - \theta_2$, including those made with ratio-based metrics $\theta > 0$ that can be expressed as a difference on the logarithmic scale. For such analyses, interval hypotheses of the form $H_1 : \theta \in (\delta_L, \delta_U)$ are routinely considered, where $-\infty \leq \delta_L < \delta_U \leq \infty$. The interval (δ_L, δ_U) accommodates the context of comparison. Assuming larger θ_j values are preferred, the intervals $(\delta_L, \delta_U) = \{(0, \infty), (-\delta, \delta), (-\delta, \infty)\}$ for an equivalence margin $\delta > 0$ may be used to respectively assess whether θ_1 is superior, practically equivalent (Spiegelhalter et al., 1994, 2004), or noninferior to θ_2 .

Decision-making methods with posterior probabilities have been proposed in a variety of settings (see e.g., Berry et al. (2011); Brutti et al. (2014); Stevens and Hagar (2022)). Given data observed from two groups, the posterior probability $Pr(H_1 | data)$ is compared to a conviction threshold $0.5 \leq \gamma < 1$. If that probability is greater than γ , one should conclude $\theta \in (\delta_L, \delta_U)$. When comparing complementary hypotheses $H_1 : \theta \in (\delta_L, \delta_U)$ and $H_0 : \theta \notin (\delta_L, \delta_U)$, decision-making methods with Bayes factors (Jeffreys, 1935; Kass and

*Luke Hagar is the corresponding author and may be contacted at lmhagar@uwaterloo.ca.

Raftery, 1995; Morey and Rouder, 2011) can be viewed as a special case of those with posterior probabilities (Hagar and Stevens, 2023). This paper therefore focuses on posterior probabilities, though the methods extend to the use of Bayes factors.

Study design often requires approximating posteriors corresponding to many hypothetical samples. In clinical trials, regulatory agencies require that Bayesian designs are assessed with respect to frequentist operating characteristics (FDA, 2019). Decision makers in industrial and corporate settings may also want to control the power and type I error rate of Bayesian designs to justify funding studies and using them to draw trustworthy conclusions. Since these design procedures leverage theory from Bayesian and frequentist statistics, they are often called hybrid approaches to sample size determination (Berry et al., 2011).

These hybrid approaches involve exploring the sampling distribution of posterior probabilities under various data generation processes. In design settings, the data have not been observed and are random variables. Data from a random sample are represented by $\mathbf{Y}^{(n,q)}$, consisting of observations $\{y_{i1}\}_{i=1}^n$ from group 1 and observations $\{y_{i2}\}_{i=1}^{\lfloor qn \rfloor}$ from group 2 for some constant $q > 0$. A *design* prior $p_D(\boldsymbol{\eta})$ (De Santis, 2007; Berry et al., 2011; Gubbiotti and De Santis, 2011) models uncertainty regarding the model parameters $\boldsymbol{\eta} = (\boldsymbol{\eta}_1, \boldsymbol{\eta}_2)$ from each group in pre-experimental settings. The characteristic of interest θ_j for group j is typically specified as a function $g(\cdot)$ of the model parameters: $\theta_j = g(\boldsymbol{\eta}_j)$ for $j = 1, 2$. Since the (informative) design prior is concentrated on θ values that are relevant to the objective of the study, it is usually different from the *analysis* prior used to analyze the observed data. The design prior gives rise to the prior predictive distribution of $\mathbf{Y}^{(n,q)}$:

$$p(\mathbf{Y}^{(n,q)}) = \int \prod_{i=1}^n f(y_{i1}; \boldsymbol{\eta}_1) \prod_{i=1}^{\lfloor qn \rfloor} f(y_{i2}; \boldsymbol{\eta}_2) p_D(\boldsymbol{\eta}) d\boldsymbol{\eta}, \quad (1)$$

where $f(y; \boldsymbol{\eta}_j)$ is the model for group $j = 1, 2$. Gubbiotti and De Santis (2011) defined the conditional and predictive approaches for specifying the prior predictive distribution of $\mathbf{Y}^{(n,q)}$. The conditional approach assigns all prior weight in $p_D(\boldsymbol{\eta})$ to a design value $\boldsymbol{\eta}^*$, whereas the predictive approach uses a nondegenerate design prior.

Various methods have been proposed to control posterior-based operating characteristics (Berry et al., 2011; Gubbiotti and De Santis, 2011; Brutti et al., 2014). To control both power and the type I error rate for a posterior analysis, it is often necessary to specify two prior predictive distributions for $\mathbf{Y}^{(n,q)}$. One typically defines the power criterion under the assumption that the hypothesis H_1 is true. The selected sample size n ensures the probability of concluding that H_1 is true is at least $1 - \beta$ for some target power $1 - \beta \in (0, 1)$:

$$\mathbb{E} [\mathbb{I}\{Pr(H_1 | \mathbf{Y}_1^{(n,q)}) \geq \gamma\}] \geq 1 - \beta, \quad (2)$$

for some conviction threshold $\gamma \in [0.5, 1)$. The criterion in (2) holds when $\mathbf{Y}_1^{(n,q)} \sim p_1(\mathbf{Y}_1^{(n,q)})$ as defined in (1) with a design prior $p_{D_1}(\boldsymbol{\eta})$ such that $p_{D_1}(H_1) = 1$.

In contrast, a criterion for the type I error rate is commonly defined by assuming that H_1 is false. To

bound the type I error rate, the selected conviction threshold γ ensures the probability of concluding that H_1 is true is at most α for some significance level $\alpha \in (0, 1)$:

$$\mathbb{E} [\mathbb{I}\{Pr(H_1 | \mathbf{Y}_0^{(n,q)}) \geq \gamma\}] \leq \alpha. \quad (3)$$

The criterion in (3) holds when $\mathbf{Y}_0^{(n,q)} \sim p_0(\mathbf{Y}_0^{(n,q)})$ as defined in (1) with a design prior $p_{D_0}(\boldsymbol{\eta})$ such that $p_{D_0}(H_1) = 0$. For design with posterior-based operating characteristics, the choice of conviction threshold $\gamma \in [0.5, 1)$ is not purely dictated by the upper bound α for the type I error rate. With a degenerate design prior $p_{D_0}(\boldsymbol{\eta})$ such that $\theta^* = g(\boldsymbol{\eta}_1^*) - g(\boldsymbol{\eta}_2^*)$ equals δ_L or δ_U , the sampling distribution of $Pr(H_1 | \mathbf{Y}_0^{(n,q)})$ converges to a uniform distribution as $n \rightarrow \infty$ under weak conditions (Golchi and Willard, 2023). In such cases, choosing $\gamma \approx 1 - \alpha$ will satisfy the criterion in (3) for large sample sizes. However, the optimal choice for γ may differ substantially from $1 - \alpha$ for moderate sample sizes or when nondegenerate design priors are used to define the prior predictive distribution of $\mathbf{Y}_0^{(n,q)}$. Although not pursued in this paper, the proposed methodology can be trivially extended to control the false discovery rate (FDR) by taking $\alpha = (1 - \beta) / (1/\text{FDR} - 1)$.

To support flexible study design, (n, γ) combinations that control posterior-based operating characteristics can be found using simulation. Most simulation-based procedures to evaluate the power criterion in (2) with design priors follow a similar process (Wang and Gelfand, 2002). First, an (n, γ) combination is selected. Second, a value $\boldsymbol{\eta}^*$ is drawn from the design prior $p_{D_1}(\boldsymbol{\eta})$. Third, data $\mathbf{y}_{*1}^{(n,q)}$ are generated according to the model $f(\mathbf{y}; \boldsymbol{\eta}^*)$. Fourth, the posterior of θ given $\mathbf{y}_{*1}^{(n,q)}$ is approximated to check if $Pr(H_1 | \mathbf{y}_{*1}^{(n,q)}) > \gamma$. This process is repeated many times to determine whether the power criterion is satisfied with probability at least $1 - \beta$ for the selected (n, γ) combination. A similar process can be repeated to evaluate whether the criterion in (3) is satisfied for a given (n, γ) combination with the design prior $p_{D_0}(\boldsymbol{\eta})$, samples $\mathbf{y}_{*0}^{(n,q)}$, and significance level α . To find a suitable design, time is wasted considering (n, γ) combinations that are suboptimal. This computational inefficiency is compounded over all combinations of the design inputs that practitioners wish to investigate – including the interval (δ_L, δ_U) , design and analysis priors, and values for α , β , and q . A fast framework to determine the (n, γ) combination that minimizes the sample size n while satisfying criteria for both posterior-based operating characteristics would mitigate this issue and enhance collaborative study design.

Recently, several strategies have been employed to reduce the computational burden associated with controlling posterior-based operating characteristics in Bayesian study design. Certain strategies are tailored to specific statistical models. For instance, Shi and Yin (2019) exploited the monotonicity of posterior probabilities as a function of the number of successful Bernoulli trials to find optimal conviction thresholds that maintained type I error rates in sequential designs. Other approaches accommodate a variety of statistical models. One such general strategy imposes parametric assumptions on the sampling distribution of posterior probabilities. Golchi (2022) fit beta distributions to approximate such sampling distributions for

various design values η^* using Gaussian processes that exploited spatial correlation between similar design inputs. [Golchi and Willard \(2023\)](#) presented an alternative method to fit those beta distributions η^* using asymptotic theory.

An alternative general strategy involves nonuniform exploration of the sampling distribution of posterior probabilities. [Hagar and Stevens \(2023\)](#) proposed such a method for power curve approximation with posterior analyses. Their method prioritizes exploring posterior probabilities such that $Pr(H_1|data) \approx \gamma$ without imposing parametric assumptions on the sampling distribution of $Pr(H_1|data)$. Their approach is useful but its simplifying assumptions may be impractical in complex design scenarios. First, [Hagar and Stevens \(2023\)](#) only considered the prior predictive distribution of $\mathbf{Y}^{(n,q)}$ under degenerate design priors. Second, their method did not jointly explore the (n, γ) -space and required complete reimplementations to consider various, user-specified γ values. Finally, they did not consider type I error rates, so the impact of the analysis priors on such rates was not well studied. Here, we overcome these limitations by generalizing their targeted exploration approach to facilitate scalable design with posterior-based operating characteristics.

The remainder of this article is structured as follows. We describe an example with genetically modified crops that involves the comparison of ordinal means in [Section 2](#). This example is referenced throughout the paper to illustrate the proposed methods. In [Section 3](#), we present a general framework to define nondegenerate design priors under the assumption that H_1 is true or false, and we choose design priors for the illustrative example. In [Section 4](#), we propose a method to determine which (n, γ) combination minimizes the sample size n while satisfying the criteria in [\(2\)](#) and [\(3\)](#). This procedure leverages a targeted exploration approach based on novel theoretical results that we prove in this paper. In [Section 5](#), we repurpose the posterior probabilities used to find the optimal (n, γ) combination to create contour plots that facilitate the investigation of various n and γ values; this process is illustrated for the example with ordinal data. We conclude with a summary and discussion of extensions to this work in [Section 6](#). Additional theoretical results and numerical studies are made available in an online supplement.

2 Illustrative Example

Since malnutrition caused by nutrient intake deficiencies is a serious concern in the African country of Malawi, the investigation of genetically modified maize (corn) varieties is prevalent. These varieties contain more provitamin A carotenoids that are converted into vitamin A during the digestion process than standard varieties. [Munkhuwa et al. \(2022\)](#) recently conducted a study at the Lilongwe University of Agriculture and Natural Resources (LUANAR) to compare an existing maize variety (MH43 A, provitamin A level: 9.3 $\mu\text{g/g}$) with a newer one (MH44 A, provitamin A level: 9.6 $\mu\text{g/g}$). While the newer maize variety boasts a higher provitamin A level, this increase will not lead to more vitamin A production if there are substantial aversions to the newer variety compared to existing ones.

The LUANAR study characterized how much children between 6 and 24 months of age enjoyed a porridge sample made with one of the two maize varieties using a Likert scale (Likert, 1932) with $w = 5$ categories. Scores of 1 and 5 respectively indicated that the child was very dissatisfied and very satisfied with the porridge sample, prompting an observation $y_{ij} \in \{1, 2, 3, 4, 5\}$ for each child $i = 1, \dots, n_j$, $j = 1, 2$. In total, $n_1 = 108$ and $n_2 = 137$ children were given porridge samples made with the MH44 A ($j = 1$) and MH43 A ($j = 2$) varieties, respectively. For group j , the multinomial distribution assumes that each participant is assigned Likert response v with probability $0 < p_{jv} < 1$ for $v = 1, \dots, w$ such that $\sum_{v=1}^w p_{jv} = 1$. Our metric of interest is $\theta_j = \mathbb{E}(y_{ij}) = \sum_{v=1}^w v p_{jv}$ for group $j = 1, 2$. We consider the new maize variety to be noninferior to the existing one when $\theta = \theta_1 - \theta_2 \in (-0.5, \infty)$, where $\delta_L = -0.5$ was chosen for illustration to reflect half of the distance between consecutive categories on this ordinal scale.

The observed sample means for the Likert data are $\hat{\theta}_1 = 4.18$ and $\hat{\theta}_2 = 4.38$. The distribution of Likert responses for each maize variety is visualized in the left plot of Figure 1. We assign uninformative Dirichlet $\text{DIR}(0.8, 0.8, 0.8, 0.8, 0.8)$ priors to $\boldsymbol{\eta}_j = \boldsymbol{p}_j = (p_{j1}, p_{j2}, \dots, p_{j5})$ for $j = 1, 2$. We obtain 10^5 posterior draws for \boldsymbol{p}_1 and \boldsymbol{p}_2 using Markov chain Monte Carlo to approximate the posterior of $\theta = \theta_1 - \theta_2$, which is illustrated in the right plot of Figure 1. The posterior probability $\Pr(\theta > -0.5 \mid \text{data}) = 0.9877$ is larger than most conventional conviction thresholds $\gamma \in [0.5, 1)$, suggesting that the new maize variety is noninferior to the old. Nevertheless, design methods that prescribe γ to control posterior-based operating characteristics prior to observing data provide a valuable framework to draw informed conclusions based on such posterior probabilities.

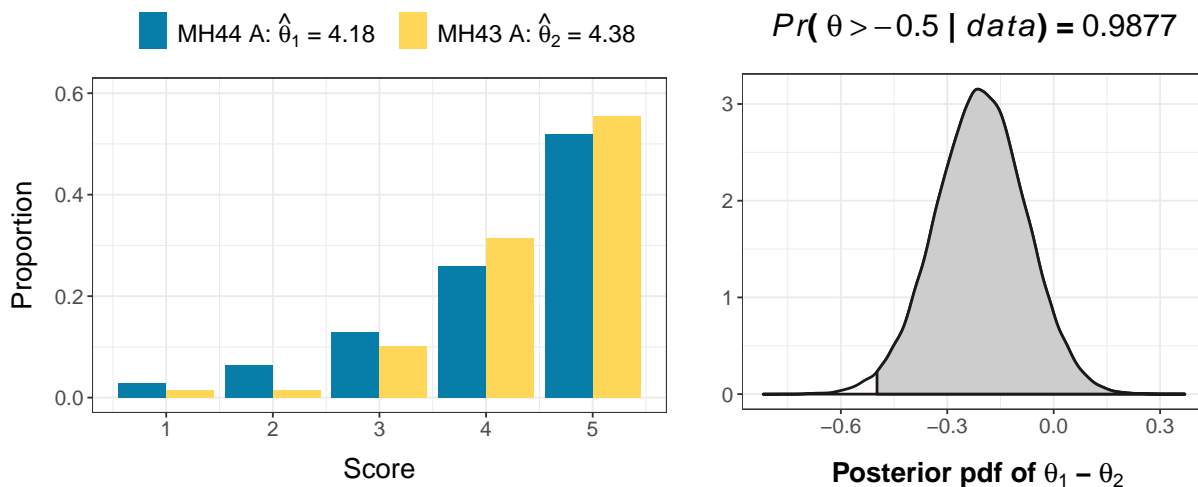


Figure 1: Left: Distribution of Likert data for each maize variety. Right: Visualization of the posterior for the difference between the ordinal means.

3 A Framework for Design Prior Specification

3.1 Design Prior Specification and Segmentation

We directly elicit priors for the model parameters $\boldsymbol{\eta}_1$ and $\boldsymbol{\eta}_2$ that indirectly induce priors on the characteristics θ_1 , θ_2 , and θ . For two-group comparisons, existing knowledge of the reference group ($j = 2$) can often be used to choose a prior $p_D(\boldsymbol{\eta}_2)$ and induce a prior $p_D(\theta_2)$ on $\theta_2 = g(\boldsymbol{\eta}_2)$. Interactive graphical interfaces are commonly used to facilitate iterative prior elicitation procedures (Chaloner, 1996; Williams et al., 2021). These interfaces provide instant feedback regarding how changes to the directly specified prior $p_D(\boldsymbol{\eta}_j)$ impact the induced prior $p_D(\theta_j)$. In Section 3.2, we demonstrate the utility of such procedures for the illustrative example. Prior specification for $\boldsymbol{\eta}_1$ and θ_1 in the comparison group ($j = 1$) is typically more difficult. However, we can often use visualization techniques along with the anticipated effect size for $\theta = \theta_1 - \theta_2$ and the prior $p_D(\boldsymbol{\eta}_2)$ to ensure the priors $p_D(\boldsymbol{\eta}_1)$ and $p_D(\theta_1)$ are suitable.

To obtain the two required design priors $p_{D_1}(\boldsymbol{\eta})$ and $p_{D_0}(\boldsymbol{\eta})$, we specify a design prior $p_D(\boldsymbol{\eta})$ for $\boldsymbol{\eta} = (\boldsymbol{\eta}_1, \boldsymbol{\eta}_2)$ that is diffuse enough to ensure that the induced prior $p_D(\theta)$ assigns nonnegligible prior weight to the interval (δ_L, δ_U) and its neighbouring regions. We respectively define $p_{D_1}(\boldsymbol{\eta})$ and $p_{D_0}(\boldsymbol{\eta})$ for the power and type I error rate criteria by segmenting the prior $p_D(\boldsymbol{\eta})$. For design purposes, we define two regions in the θ -space to carry out this segmentation. The first region $\mathcal{G} = \{(G_L, G_U) : \delta_L \leq G_L < G_U \leq \delta_U\}$ pertains to the power criterion in (2), where $\theta \in \mathcal{G}$ ensures that $H_1 : \theta \in (\delta_U, \delta_L)$ is true. The second region $\mathcal{R} = \{(R_{1L}, R_{1U}] \cup [R_{2L}, R_{2U}) : R_{1L} < R_{1U} \leq \delta_L < \delta_U \leq R_{2L} < R_{2U}\}$ pertains to the criterion for the type I error rate in (3). The region \mathcal{R} is defined to accommodate interval hypotheses based on practical equivalence where both $\theta < \delta_L$ and $\theta > \delta_U$ are undesirable outcomes. When either δ_L or δ_U is not finite, the region \mathcal{R} can be expressed as a single region $\mathcal{R} = \{(R_L, R_U] : R_L < R_U \leq \delta_L \vee [R_L, R_U) : \delta_U \leq R_L < R_U\}$. For either scenario, the hypothesis H_1 is false when $\theta \in \mathcal{R}$. In this work, we refer to the regions \mathcal{G} and \mathcal{R} as the *green* and *red* regions of the θ -space, respectively. Further details concerning the definition of these regions are provided in Section 3.2.

One method to define the design priors $p_{D_1}(\boldsymbol{\eta})$ and $p_{D_0}(\boldsymbol{\eta})$ involves truncating the more diffuse prior $p_D(\boldsymbol{\eta})$ according to the regions \mathcal{G} and \mathcal{R} such that $p_{D_1}(\boldsymbol{\eta}) \propto p_D(\boldsymbol{\eta})\mathbb{I}(\theta \in \mathcal{G})$ and $p_{D_0}(\boldsymbol{\eta}) \propto p_D(\boldsymbol{\eta})\mathbb{I}(\theta \in \mathcal{R})$. Since we can readily sample from $p_D(\boldsymbol{\eta})$, rejection sampling methods (Casella et al., 2004) allow us to obtain samples from $p_{D_1}(\boldsymbol{\eta})$ and $p_{D_0}(\boldsymbol{\eta})$. Alternatively, we could define design priors such that $p_{D_1}(\boldsymbol{\eta}) \propto p_D(\boldsymbol{\eta}|\theta \sim \mathcal{U}(\mathcal{G}))$ and $p_{D_0}(\boldsymbol{\eta}) \propto p_D(\boldsymbol{\eta}|\theta \sim \mathcal{U}(\mathcal{R}))$, where $\mathcal{U}(\cdot)$ indicates that θ is uniformly distributed over that region. These design priors provide a mechanism for obtaining parameter values $\boldsymbol{\eta}$ corresponding to particular regions of the θ -space that de-emphasizes the shape of the induced prior $p_D(\theta)$. For these design priors, we can use sampling-resampling methods (Rubin, 1988; Smith and Gelfand, 1992) to obtain a sample from $p_{D_1}(\boldsymbol{\eta})$ or $p_{D_0}(\boldsymbol{\eta})$ given a sample from $p_D(\boldsymbol{\eta})$. This sampling-resampling approach is the one we employ in this paper, but a host of other methods could also be used to choose the design priors $p_{D_1}(\boldsymbol{\eta})$ and $p_{D_0}(\boldsymbol{\eta})$. We recommend

consulting the literature on prior elicitation if alternative prior specification methods are required (Chaloner, 1996; Garthwaite et al., 2005).

3.2 Design Priors for the Illustrative Example

For the multinomial model used in Section 2, it is not trivial to choose an informative prior for $\boldsymbol{\eta}_j = \mathbf{p}_j$ that enforces the unit-sum constraint $\sum_{v=1}^w p_{jv} = 1$. We instead assign a joint prior to variables obtained with an invertible transformation from Elfadaly and Garthwaite (2017):

$$Z_{j1} = p_{j1}, \quad Z_{jv} = \frac{p_{jv}}{1 - \sum_{t=1}^{v-1} p_{jt}} \quad \text{for } v = 2, \dots, w-1, \quad \text{and} \quad Z_{jw} = 1, \quad (4)$$

for groups $j = 1, 2$. The variable Z_{jv} represents the probability that an observation from group j is assigned to category v given that it has not been assigned to categories $1, \dots, v-1$. We assign independent marginal $\text{BETA}(\alpha_{jv}, \beta_{jv})$ priors to Z_{jv} , $v = 1, \dots, w-1$ to induce a joint prior on \mathbf{p}_j that satisfies the unit-sum constraint.

This interactive graphical interface was developed and used to specify design priors for the illustrative example: https://luke-hagar.shinyapps.io/Ordinal_Priors/. We use this interface as described in Appendix C.1 of the supplement to specify the following marginal priors for the reference group: $\text{BETA}(2.20, 123.29)$ for Z_{21} , $\text{BETA}(2.15, 118.50)$ for Z_{22} , $\text{BETA}(3.43, 29.87)$ for Z_{23} , and $\text{BETA}(6.67, 12.16)$ for Z_{24} . These priors jointly induce a design prior on θ_2 that is visualized in the center plot of Figure 2. The prior median of 4.38 coincides with the observed ordinal mean for the reference group. To specify $p_D(\boldsymbol{\eta}_1)$ for the comparison group, we consider the reference data and observed effect size of -0.2 , which serves as an anticipated effect size for this illustration. We implement the process from Appendix C.1 to specify the following marginal priors for the comparison group: $\text{BETA}(1.99, 56.22)$ for Z_{11} , $\text{BETA}(3.16, 66.19)$ for Z_{12} , $\text{BETA}(5.61, 34.18)$ for Z_{13} , and $\text{BETA}(11.66, 19.45)$ for Z_{14} . The induced design prior on θ_1 with prior median of 4.18 is visualized in left plot of Figure 2. Under the assumption that $\boldsymbol{\eta}_1$ and $\boldsymbol{\eta}_2$ are independent, the induced prior on θ is depicted in the right plot of Figure 2.

We now provide general guidance for choosing the regions \mathcal{G} and \mathcal{R} , and we overview how the recommended (n, γ) combination depends on these choices. We focus on the case where one of δ_L or δ_U is not finite, but this guidance can be extended to settings where $-\infty < \delta_L < \delta_U < \infty$. First, we advise that \mathcal{G} and \mathcal{R} be chosen as noncontiguous regions so that the study aims to detect meaningful effects. If $G_L = R_U + \epsilon$ or $R_L = G_U + \epsilon$ for some small $\epsilon > 0$, then impractically large sample sizes n may be required to discern miniscule differences between $\theta \in \mathcal{R}$ and $\theta \in \mathcal{G}$. We recommend choosing \mathcal{R} to be contiguous with the interval (δ_L, δ_U) . We recommend centering \mathcal{G} around an anticipated or meaningful value for $\theta \in (\delta_L, \delta_U)$ such that discerning differences between $\theta \in \mathcal{G}$ and $\theta \notin (\delta_L, \delta_U)$ is important, where there is sufficient distance between the endpoints of \mathcal{G} and (δ_L, δ_U) .

If $R_L \ll R_U < \delta_L$ or $R_U \gg R_L > \delta_U$, the optimal conviction threshold γ typically approaches 0.5 as

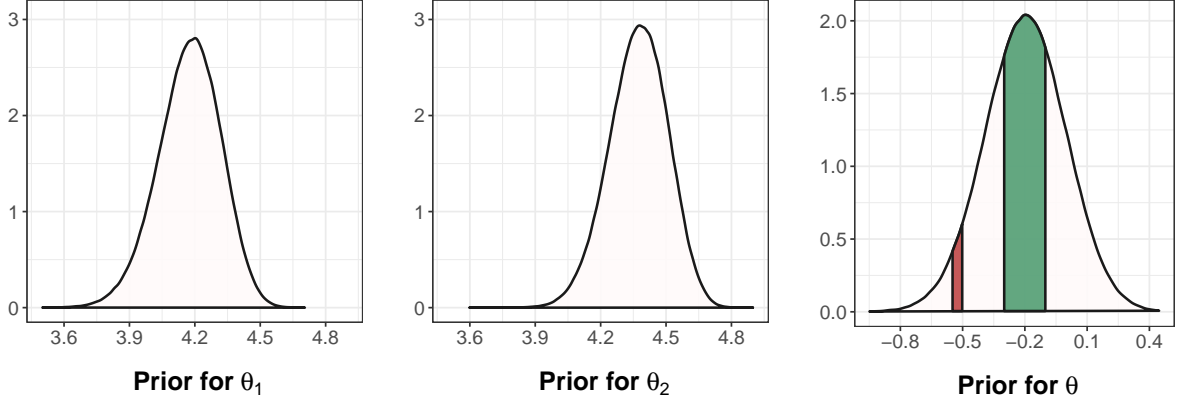


Figure 2: Induced design priors for θ_1 (left), θ_2 (center), and θ (right). The green and red regions of the θ -space are visualized on the right plot.

the sample size n increases because $Pr(H_1 | \mathbf{Y}_1^{(n,q)}) \rightarrow 1$ and $Pr(H_1 | \mathbf{Y}_0^{(n,q)}) \rightarrow 0$. With smaller values for $\gamma \in [0.5, 1)$, we require less evidence to support H_1 ; however, specifying a wide interval for \mathcal{R} will lead to an inflated type I error rate if we are truly only concerned with controlling type I error for θ values that are *just* outside the interval (δ_L, δ_U) . As such, we generally recommend specifying \mathcal{R} to be a narrow interval that is contiguous with (δ_L, δ_U) . These recommendations are applied with the the illustrative example in Section 2: the region $\mathcal{G} = (-0.3, -0.1)$ is centered at the anticipated effect size of -0.2 , and $\mathcal{R} = (-0.55, -0.5)$ is contiguous with the interval $(\delta_L, \delta_U) = (-0.5, \infty)$ defined previously. These red and green regions are depicted on the prior for θ in the right plot of Figure 2.

4 Design with Multiple Operating Characteristics

4.1 Mapping the Sampling Distribution of Posterior Probabilities to Low-Dimensional Hypercubes

Design methods with posterior-based operating characteristics require that we explore the sampling distribution of posterior probabilities for various sample sizes n . Here, we extend methods from Hagar and Stevens (2023) to improve computational complexity by mapping these sampling distributions to low-dimensional hypercubes $[0, 1]^{2d}$, where the model $f(y; \boldsymbol{\eta}_j)$ is parameterized by $\boldsymbol{\eta}_j \in \mathbb{R}^d$. Given parameter values $\boldsymbol{\eta}_1^*$ and $\boldsymbol{\eta}_2^*$, each observation in $\mathbf{y}^{(n,q)}$ is typically simulated using cumulative distribution function (CDF) inversion with one coordinate of the point $\mathbf{u} \in [0, 1]^{n_1+n_2}$. We typically have that $2d \ll n_1 + n_2$, and this dimension reduction allows us to estimate posterior-based operating characteristics using only a subspace of $[0, 1]^{2d}$ in Section 4.2.

Our design framework assumes that data $\{y_{i1}\}_{i=1}^{n_1}$ and $\{y_{i2}\}_{i=1}^{n_2}$ are to be collected independently, where the data generation process for samples of size $n_1 = n$ and $n_2 = \lfloor qn \rfloor$ is characterized by the procedure detailed in Section 1. That is, data from group j are generated from the model $f(y; \boldsymbol{\eta}_j^*)$, where the parameter

values $\boldsymbol{\eta}^* = (\boldsymbol{\eta}_1^*, \boldsymbol{\eta}_2^*)$ are drawn from the relevant design prior. These parameter values specify anticipated values $\theta_j^* = g(\boldsymbol{\eta}_j^*)$ for the characteristics of interest and their difference $\theta^* = \theta_1^* - \theta_2^*$.

To broadly map posterior probabilities to low-dimensional hypercubes, we can generate maximum likelihood estimates $\hat{\boldsymbol{\eta}}_{1,n_1}$ and $\hat{\boldsymbol{\eta}}_{2,n_2}$ instead of data $\mathbf{y}^{(n,g)}$. For sufficiently large sample sizes, the MLEs $\hat{\boldsymbol{\eta}}_{j,n_j}$ approximately and independently follow $\mathcal{N}(\boldsymbol{\eta}_j^*, \mathcal{I}^{-1}(\boldsymbol{\eta}_j^*)/n_j)$ distributions, $j = 1, 2$. We require a sequence of m points $\{\mathbf{u}_r\}_{r=1}^m \in [0, 1]^{2d}$ to simulate from the joint limiting distribution of $\hat{\boldsymbol{\eta}}_{1,n_1}$ and $\hat{\boldsymbol{\eta}}_{2,n_2}$, where each point corresponds to a simulation repetition. We can use these maximum likelihood estimates for posterior approximation when the models $f(y; \boldsymbol{\eta}_1)$ and $f(y; \boldsymbol{\eta}_2)$ belong to the exponential family (Lehmann and Casella, 1998). We accommodate posterior approximation for models that are not in the exponential family in Appendix D of the supplement.

For models $f(y; \boldsymbol{\eta}_j)$ in the exponential family, the first derivative of the log-likelihood with respect to $\eta_{j,k}$, the k^{th} component of $\boldsymbol{\eta}_j$, takes the form

$$\frac{\partial}{\partial \eta_{j,k}} \log \left[\prod_{i=1}^{n_j} f(y_{ij}; \boldsymbol{\eta}_j) \right] = n \frac{\partial}{\partial \eta_{j,k}} A(\boldsymbol{\eta}_j) + \sum_{s=1}^d \frac{\partial}{\partial \eta_{j,k}} C_s(\boldsymbol{\eta}_j) \sum_{i=1}^{n_j} T_s(y_{ij}), \quad (5)$$

where $A(\boldsymbol{\eta}_j)$, $C_s(\boldsymbol{\eta}_j)$, and $T_s(y)$ are known functions for $s = 1, \dots, d$. For group j , $T_{j\ddagger}(\mathbf{y}^{(n,g)}) = (\sum_{i=1}^{n_j} T_1(y_{ij}), \dots, \sum_{i=1}^{n_j} T_s(y_{ij}))$ are sufficient statistics that provide as much information about the parameter $\boldsymbol{\eta}_j$ as the entire sample $\mathbf{y}^{(n,g)}$. At the maximum likelihood estimate $\hat{\boldsymbol{\eta}}_{j,n_j}$, all d partial derivatives in (5) equal 0. All components of $T_{j\ddagger}(\mathbf{y}^{(n,g)})$ can be recovered by substituting the maximum likelihood estimate $\hat{\boldsymbol{\eta}}_{j,n_j}$ into the system of linear equations in (5). Given analysis priors $p_1(\boldsymbol{\eta}_1)$ and $p_2(\boldsymbol{\eta}_2)$, we use the Laplace approximation to the posterior that is centered at the posterior mode $\tilde{\boldsymbol{\eta}}_{j,n_j} = \arg \max_{\boldsymbol{\eta}_j} p_j(\boldsymbol{\eta}_j | \text{data})$ for $j = 1$ and 2 (Gelman et al., 2013). The multivariate delta method prompts the following large-sample approximation to the posterior of θ :

$$\mathcal{N} \left(g(\tilde{\boldsymbol{\eta}}_{1,n_1}) - g(\tilde{\boldsymbol{\eta}}_{2,n_2}), \sum_{j=1}^2 \left[\frac{\partial g^T}{\partial \boldsymbol{\eta}} \mathcal{J}_j(\boldsymbol{\eta})^{-1} \frac{\partial g}{\partial \boldsymbol{\eta}} \right]_{\boldsymbol{\eta}=\tilde{\boldsymbol{\eta}}_{j,n_j}} \right) \quad \text{for } \mathcal{J}_j(\boldsymbol{\eta}) = -\frac{\partial^2}{\partial \boldsymbol{\eta}^2} \log(p_j(\boldsymbol{\eta} | \text{data})). \quad (6)$$

Algorithm 1 details how we use a single point $\mathbf{u} \in [0, 1]^{2d}$ to obtain the posterior approximation in (6), where $\hat{\eta}_{j,n_j,k}$ and $\eta_{j,k}^*$ denote the k^{th} component of their vectors. We require that the conditions for the Bernstein-von Mises (BvM) theorem hold to ensure the process to generate maximum likelihood estimates in Algorithm 1 is valid. The four necessary assumptions to invoke the BvM theorem (van der Vaart, 1998) are detailed in Appendix A.1 of the supplement. The first three assumptions are weaker than the regularity conditions for the asymptotic normality of the maximum likelihood estimator (MLE) (Lehmann and Casella, 1998), which are listed in Appendix A.2. The final assumption for the BvM theorem requires that the prior distribution of $\boldsymbol{\eta}_j$ be continuous in a neighbourhood of $\boldsymbol{\eta}_j^*$ with positive density for $j = 1, 2$. In Appendix C.2, we propose an alternative method to obtain $T_{1\ddagger}(\mathbf{y}^{(n,g)})$ and $T_{2\ddagger}(\mathbf{y}^{(n,g)})$ from $\mathbf{u} \in [0, 1]^{2d}$ that is useful when the distributions of $\hat{\boldsymbol{\eta}}_{1,n_1}$ and $\hat{\boldsymbol{\eta}}_{2,n_2}$ are not approximately normal for moderate sample sizes. That

method is based on linear approximations to the CDF of $T_{j^\dagger}(\mathbf{y}^{(n,q)})$ for discrete models in the exponential family.

Algorithm 1 Low-Dimensional Posterior Approximation

- 1: **procedure** APPROXIMATE($f(y; \boldsymbol{\eta}_1^*), f(y; \boldsymbol{\eta}_2^*), g(\cdot), n, q, \mathbf{u}, p_1(\boldsymbol{\eta}_1), p_2(\boldsymbol{\eta}_2)$)
 - 2: **for** j in $\{1, 2\}$ **do**
 - 3: **for** k in $1:d$ **do**
 - 4: Let $\hat{\eta}_{j,n_j,k}(\mathbf{u})$ be the $u_{(j-1)d+k}$ -quantile of $\mathcal{N}(\eta_{j,k}^*, \mathcal{I}(\eta_{j,k}^*)^{-1}/n_j)$ conditional on $\hat{\eta}_{j,n_j,0}(\mathbf{u}), \dots, \hat{\eta}_{j,n_j,k-1}(\mathbf{u})$.
 - 5: Solve the system of equations in (5) with $\boldsymbol{\eta}_j = \hat{\boldsymbol{\eta}}_{j,n_j}(\mathbf{u})$ to obtain $T_{j^\dagger}(\mathbf{y}^{(n,q)})$.
 - 6: Use $T_{j^\dagger}(\mathbf{y}^{(n,q)})$ to obtain the posterior mode $\tilde{\boldsymbol{\eta}}_{j,n_j}$ via optimization.
 - 7: Use $\tilde{\boldsymbol{\eta}}_{1,n_1}(\mathbf{u}), \tilde{\boldsymbol{\eta}}_{2,n_2}(\mathbf{u}), T_{1^\dagger}(\mathbf{y}^{(n,q)}), T_{2^\dagger}(\mathbf{y}^{(n,q)})$, and $g(\cdot)$ to obtain (6).
-

For concision, we let $\mathcal{N}(\underline{\theta}_r^{(n,q)}, \underline{\tau}_r^{(n,q)})$ denote the approximation to the posterior of θ in (6) corresponding to the point $\mathbf{u}_r \in [0, 1]^{2d}$ and sample sizes $n_1 = n$ and $n_2 = \lfloor qn \rfloor$ for $r = 1, \dots, m$. The mean $\underline{\theta}_r^{(n,q)}$ and variance $\underline{\tau}_r^{(n,q)}$ of this approximation are implicit functions of n . The estimate for the posterior probability $Pr(\theta < \delta \mid \text{data})$ is then

$$p_{n,q,\mathbf{u}_r}^\delta = \Phi\left(\frac{\delta - \underline{\theta}_r^{(n,q)}}{\sqrt{\underline{\tau}_r^{(n,q)}}}\right), \quad (7)$$

where $\Phi(\cdot)$ is the CDF of the standard normal distribution. The estimates from (7) comprise the sampling distributions of posterior probabilities after mapping to $[0, 1]^{2d}$. These distributions should accurately approximate the exact sampling distribution of posterior probabilities; Theorem 1 demonstrates that the exact sampling distribution of posterior probabilities induced by (6) with data $\mathbf{Y}^{(n,q)}$ converges to the sampling distribution prompted by Algorithm 1 with pseudorandom sequences as $n \rightarrow \infty$. We emphasize that Theorem 1 applies to the sampling distribution of posterior probabilities when $\boldsymbol{\eta}^* \sim p_{D_1}(\boldsymbol{\eta})$ as in (2) or when $\boldsymbol{\eta}^* \sim p_{D_0}(\boldsymbol{\eta})$ as in (3).

Theorem 1. *Let $\boldsymbol{\eta}^* = (\boldsymbol{\eta}_1^*, \boldsymbol{\eta}_2^*) \sim p_D(\boldsymbol{\eta})$ for some design prior $p_D(\boldsymbol{\eta})$ such that the following conditions hold for all $\boldsymbol{\eta}^*$ with $p_D(\boldsymbol{\eta}^*) > 0$. Let $f(y; \boldsymbol{\eta}_1^*)$ and $f(y; \boldsymbol{\eta}_2^*)$ satisfy the regularity conditions from Appendix A.2. Let the prior $p_j(\boldsymbol{\eta}_j)$ be continuous in a neighbourhood of $\boldsymbol{\eta}_j^*$ with positive density for $j = 1, 2$. Let $g(\boldsymbol{\eta})$ be differentiable at $\boldsymbol{\eta}_j^*$ for $j = 1, 2$ with nonzero derivatives. Let $\mathbf{U} \stackrel{i.i.d.}{\sim} \mathcal{U}([0, 1]^{2d})$ and $\mathbf{Y}^{(n,q)}$ be generated independently from $f(y; \boldsymbol{\eta}_1^*)$ and $f(y; \boldsymbol{\eta}_2^*)$. Let $\mathcal{P}_{n,q,\Pi,\zeta}^\delta$ denote the sampling distribution of posterior probabilities for $Pr(\theta < \delta \mid \text{data})$ given sample sizes $n_1 = n$ and $n_2 = \lfloor qn \rfloor$ produced using input Π with method ζ . Then, $\mathcal{P}_{n,q,\mathbf{Y}^{(n,q)},(6)}^\delta \xrightarrow{d} \mathcal{P}_{n,q,\mathbf{U},Alg.1}^\delta$.*

The proof of Theorem 1 is given in Appendix A.3 of the supplement. We can improve upon this procedure by using low-discrepancy sequences instead of pseudorandom ones (as suggested in Theorem 1) to estimate power and the type I error rate more precisely. We use a particular class of low-discrepancy sequences called Sobol' sequences (Sobol', 1967) that induce negative dependence between the points $\mathbf{U}_1, \dots, \mathbf{U}_m$. When using randomized Sobol' sequences (Lemieux, 2009), each point in the sequence is such that $\mathbf{U}_r \sim \mathcal{U}([0, 1]^{2d})$ for

$r = 1, \dots, m$. It follows that randomized Sobol' sequences can be used similarly to pseudorandom sequences in Monte Carlo simulation to prompt unbiased estimators:

$$\mathbb{E} \left(\frac{1}{m} \sum_{r=1}^m \Psi(\mathbf{U}_r) \right) = \int_{[0,1]^{2d}} \Psi(\mathbf{u}) d\mathbf{u}, \quad (8)$$

for some function $\Psi(\cdot)$. Due to the negative dependence between the points, the variance of the estimator in (8) is typically reduced by using low-discrepancy sequences. Low-discrepancy sequences give rise to effective variance reduction methods when the dimension of the simulation is moderate. With Sobol' sequences, we can therefore use fewer simulation repetitions m to estimate posterior-based operating characteristics as detailed in Corollary 1. This corollary follows directly from Theorem 1 and (8).

Corollary 1. *Let $p_{n,q,\mathbf{u}_r}^\delta$ from (7) be the estimate for $\Pr(\theta < \delta \mid \text{data})$ corresponding to sample sizes $n_1 = n$ and $n_2 = \lfloor qn \rfloor$ and point $\mathbf{u}_r \in [0, 1]^{2d}$. Let $p_{n,q,\mathbf{u}_r}^{\delta_U - \delta_L} = p_{n,q,\mathbf{u}_r}^{\delta_U} - p_{n,q,\mathbf{u}_r}^{\delta_L}$ for $\delta_L < \delta_U$. Under the conditions for Theorem 1 as $n \rightarrow \infty$, power in (2) and the type I error rate in (3) are consistently estimated by*

$$\frac{1}{m} \sum_{r=1}^m \mathbb{I}(p_{n,q,\mathbf{u}_r}^{\delta_U - \delta_L} \geq \gamma),$$

when $\{\mathbf{U}_r\}_{r=1}^m$ are generated using pseudorandom or randomized Sobol' sequences.

Corollary 1 ensures that Algorithm 1 with randomized Sobol' sequences gives rise to consistent estimators for power and the type I error rate as $n \rightarrow \infty$ when the hypercube $[0, 1]^{2d}$ is thoroughly explored. However, it does not guarantee that these estimators are unbiased for finite n . In practice, we may require fewer observations for the approximate distributions of the MLEs to be approximately normal if we consider some transformation of $\boldsymbol{\eta}_j$, particularly if any of its parameters do not have support on \mathbb{R} . Similarly, the posterior of a monotonic transformation of θ may need to be considered for the normal approximation in (6) to be suitable for moderate n . Rather than introduce new notation for these untransformed and transformed variables, we assume that $\boldsymbol{\eta}_1$, $\boldsymbol{\eta}_2$, and θ are specified to improve the quality of the normal approximation in (6).

4.2 Estimating Operating Characteristics with Segments of the Sampling Distribution

We now propose a method for targeted exploration of the sampling distribution of posterior probabilities. This novel method presented in Algorithm 2 allows us to estimate posterior-based operating characteristics without the need to explore points from throughout $[0, 1]^{2d}$ to estimate *entire* sampling distributions of posterior probabilities. This method is the main contribution of this paper, and we use it to consistently explore (n, γ) combinations with only a subset of the points $\mathbf{u}_r \in [0, 1]^{2d+1}$, $r = 1, \dots, m$. As described later in Algorithm 2, we add an extra dimension to the hypercube so that we can sample $\boldsymbol{\eta}^*$ from the relevant design prior $p_D(\boldsymbol{\eta})$. It is using only a subset of points to explore most designs that greatly enhances the scalability of our method.

The mapped posterior probabilities $p_{n,q,\mathbf{u}_r}^\delta$ depend on the models $f(y; \boldsymbol{\eta}_1^*)$ and $f(y; \boldsymbol{\eta}_2^*)$, the sample size n , and the Sobol' sequence point \mathbf{u}_r , $r = 1, \dots, m$. Standard practice fixes the sample size n and varies the point $\mathbf{u}_r \in [0, 1]^{2d+1}$ to estimate power and the type I error rate. We now fix the point \mathbf{u}_r and let the sample size n vary. When the point \mathbf{u}_r and models $f(y; \boldsymbol{\eta}_j^*)$ are fixed, $p_{n,q,\mathbf{u}_r}^\delta$ is a deterministic function of n . Lemma 1 motivates our approach to explore $[0, 1]^{2d+1}$ in a targeted manner for each sample size n explored.

Lemma 1. *Let the conditions for Theorem 1 be satisfied and define $\text{logit}(x) = \log(x) - \log(1 - x)$. For a given point $\mathbf{u}_r = (u_1, \dots, u_{2d+1}) \in [0, 1]^{2d+1}$, we have that Algorithm 1 prompts*

(a) $p_{n,q,\mathbf{u}_r}^\delta \approx \Phi(a(\delta, \theta^*)\sqrt{n} + b(\mathbf{u}_r))$ for sufficiently large n , where θ^* is the anticipated value for θ and $a(\cdot)$ and $b(\cdot)$ are functions that do not depend on n .

(b) $\lim_{n \rightarrow \infty} \frac{d}{dn} \text{logit}[\Phi(a(\delta_U, \theta^*)\sqrt{n} + b(\mathbf{u}_r)) - \Phi(a(\delta_L, \theta^*)\sqrt{n} + b(\mathbf{u}_r))]$ is $\min\{a(\delta_U, \theta^*)^2, a(\delta_L, \theta^*)^2\}/2$ when $\theta^* \in [\delta_L, \delta_U]$ and $-\min\{a(\delta_U, \theta^*)^2, a(\delta_L, \theta^*)^2\}/2$ otherwise.

We prove Lemma 1 in Appendix B of the supplement and now consider its practical implications. Lemma 1 suggests that the linear approximation to $\text{logit}(p_{n,q,\mathbf{u}_r}^{\delta_U - \delta_L})$ as a function of n is a good global approximation for sufficiently large sample sizes. Moreover, this linear approximation should be locally suitable for a range of sample sizes. These linear approximations disclose which points $\mathbf{u}_r \in [0, 1]^{2d+1}$ correspond to posterior probabilities that are in a neighbourhood of the β -quantile of the sampling distribution for the design prior $p_{D_1}(\boldsymbol{\eta})$ specified in (2). Likewise, those approximations reveal which points $\mathbf{u}_r \in [0, 1]^{2d+1}$ correspond to posterior probabilities that are in a neighbourhood of the $(1 - \alpha)$ -quantile of the sampling distribution for $p_{D_0}(\boldsymbol{\eta})$ specified in (3). This knowledge allows us to explore the sampling distributions of posterior probabilities in a targeted manner. Lemma 1 is original to this paper. Hagar and Stevens (2023) proved that $p_{n,q,\mathbf{u}_r}^{\delta_U - \delta_L}$ was increasing for sufficiently large n when $\theta^* \in (\delta_L, \delta_U)$. They used that fact to prioritize exploring posterior probabilities such that $Pr(H_1 | \text{data}) \approx \gamma$. However, their approach is of limited use when the conviction threshold γ is not predetermined.

Algorithm 2 allows users to *jointly* explore the (n, γ) -space in a targeted manner to find the (n, γ) combination that minimizes the sample size while satisfying the criteria in (2) and (3). This flexibility is crucial for design with posterior-based operating characteristics. To implement our approach, we must choose the length of the Sobol' sequence m and a constant $m_0 \ll m$. We use $m = 8192$ and $m_0 = 512$ to balance the computational efficiency and precision of the estimates for the operating characteristics. Algorithm 2 leverages order statistics, and we abbreviate the term order statistic as OS. Our approach involves thorough exploration of sampling distributions of posterior probabilities at three sample sizes – $n^{(0)}$, $n^{(1)}$, and $n^{(2)}$ – and targeted exploration for all other values of n .

We now elaborate on several of the steps in Algorithm 2. In Line 4, we use the first coordinate of each point $\mathbf{u}_{r,1}^{(h)}$ to reorder the draws in $\boldsymbol{\eta}^{*(0)}$ and $\boldsymbol{\eta}^{*(1)}$ with respect to the anticipated $\boldsymbol{\eta}$ value for $\theta = g(\boldsymbol{\eta}_1) - g(\boldsymbol{\eta}_2)$. This reordering is beneficial because we utilize only the first m_0 points from $\{\mathbf{u}_r^{(h)}\}_{r=1}^m$, $h = 0, 1$ to find an

Algorithm 2 Procedure to Determine Optimal Sample Size and Conviction Threshold

- 1: **procedure** OPTIMIZE($f(y; \boldsymbol{\eta})$, $g(\cdot)$, $p_j(\boldsymbol{\eta}_j)$, $p_{D_1}(\boldsymbol{\eta})$, $p_{D_0}(\boldsymbol{\eta})$, (δ_L, δ_U) , q , β , α , m , m_0)
 - 2: **for** h in $\{0, 1\}$ **do**
 - 3: Generate a sample $\boldsymbol{\eta}^{*(h)} \sim p_{D_h}(\boldsymbol{\eta})$ of size m and Sobol' sequence $\{\mathbf{u}_r^{(h)}\}_{r=1}^m$
 - 4: Reorder $\boldsymbol{\eta}^{*(h)}$ so its r^{th} realization prompts the $\lceil m\mathbf{u}_{r,1}^{(h)} \rceil^{\text{th}}$ OS of $g(\boldsymbol{\eta}_1^{*(h)}) - g(\boldsymbol{\eta}_2^{*(h)})$
 - 5: Use Algorithm 1 with $\{\mathbf{u}_r^{(1)}\}_{r=1}^{m_0}$ and $\{\mathbf{u}_r^{(0)}\}_{r=1}^{m_0}$ to obtain the smallest $n^{(0)}$ such that the $\lfloor m_0\beta \rfloor^{\text{th}}$ OS of $p_{n^{(0)}, q, \mathbf{u}_r^{(1)}}^{\delta_U - \delta_L} \geq$ the $\lceil m_0(1 - \alpha) \rceil^{\text{th}}$ OS of $p_{n^{(0)}, q, \mathbf{u}_r^{(0)}}^{\delta_U - \delta_L}$ via binary search
 - 6: Compute $p_{n^{(0)}, q, \mathbf{u}_r^{(1)}}^{\delta_U - \delta_L}$ for $\{\mathbf{u}_r^{(1)}\}_{r=m_0}^m$ and $p_{n^{(0)}, q, \mathbf{u}_r^{(0)}}^{\delta_U - \delta_L}$ for $\{\mathbf{u}_r^{(0)}\}_{r=m_0}^m$ via Algorithm 1
 - 7: $n^{(1)} \leftarrow 0.9n^{(0)} + 0.2n^{(0)} \mathbb{I}(\lfloor m\beta \rfloor^{\text{th}} \text{ OS of } p_{n^{(0)}, q, \mathbf{u}_r^{(1)}}^{\delta_U - \delta_L} \geq \lceil m(1 - \alpha) \rceil^{\text{th}} \text{ OS of } p_{n^{(0)}, q, \mathbf{u}_r^{(0)}}^{\delta_U - \delta_L})$
 - 8: **for** r in $1:m$ **do**
 - 9: **for** h in $\{0, 1\}$ **do**
 - 10: Compute $p_{n^{(1)}, q, \mathbf{u}_r^{(h)}}^{\delta_U - \delta_L}$ to approximate $\text{logit}(p_{n, q, \mathbf{u}_r^{(h)}}^{\delta_U - \delta_L})$ as a linear function of n
 - 11: Find the smallest $n^{(2)}$ such that the $\lfloor m\beta \rfloor^{\text{th}}$ OS of $p_{n^{(2)}, q, \mathbf{u}_r^{(1)}}^{\delta_U - \delta_L} \geq$ the $\lceil m(1 - \alpha) \rceil^{\text{th}}$ OS of $p_{n^{(2)}, q, \mathbf{u}_r^{(0)}}^{\delta_U - \delta_L}$ via binary search, where each n value is considered with only the m_0 points from $\{\mathbf{u}_r^{(h)}\}_{r=1}^{m_0}$ such that $\hat{p}_{n, q, \mathbf{u}_r^{(h)}}^{\delta_U - \delta_L}$ from Line 10 is nearest to the relevant OS
 - 12: **for** r in $1:m$ **do**
 - 13: Compute $p_{n^{(2)}, q, \mathbf{u}_r^{(1)}}^{\delta_U - \delta_L}$ and $p_{n^{(2)}, q, \mathbf{u}_r^{(0)}}^{\delta_U - \delta_L}$ via Algorithm 1 if not computed in Line 11
 - 14: **return** $n^{(2)}$ as recommended n and the $\lceil m(1 - \alpha) \rceil^{\text{th}}$ OS of $p_{n^{(2)}, q, \mathbf{u}_r^{(0)}}^{\delta_U - \delta_L}$ as γ
-

initial sample size $n^{(0)}$ in Line 5. Because subsequences of the Sobol' sequence are also low discrepancy, this reordering guarantees that the anticipated values for θ corresponding to the first m_0 points are evenly distributed over \mathcal{G} and \mathcal{R} . For the r^{th} point in the sequence for hypothesis h , we obtain the posterior approximation for (7) via Algorithm 1, where the inputs $\boldsymbol{\eta}^*$ and $\mathbf{u} \in [0, 1]^{2d}$ are respectively the r^{th} realization of $\boldsymbol{\eta}^{*(h)}$ and the final $2d$ components of $\mathbf{u}_r^{(h)}$. The inequality for the order statistics of the two sampling distributions in Line 5 must hold true for there to exist a conviction threshold γ such that the criteria in both (2) and (3) are satisfied.

We approximate $\text{logit}(p_{n, q, \mathbf{u}_r^{(h)}}^{\delta_U - \delta_L})$ as a linear function of n to efficiently explore sample sizes. To obtain this approximation for finite n , we do not use the first derivatives from part (b) of Lemma 1 prompted by limiting results. We instead construct this approximation by estimating the probabilities that correspond to $\{\mathbf{u}_r^{(0)}\}_{r=1}^{m_0}$ and $\{\mathbf{u}_r^{(1)}\}_{r=1}^{m_0}$ for the sample size $n^{(1)}$. This sample size is chosen to be larger or smaller than $n^{(0)}$ depending on the indicator function in Line 7. Once the linear approximations are obtained in Lines 8 to 10, we find the optimal (n, γ) combination in Line 11. We find the optimal design by exploring sample sizes with binary search. However, we leverage Lemma 1 to determine whether a value for n is suitable using a subset of m_0 points from each of $\{\mathbf{u}_r^{(0)}\}_{r=1}^{m_0}$ and $\{\mathbf{u}_r^{(1)}\}_{r=1}^{m_0}$.

Unlike in Line 5, we choose these points in a targeted way from each sequence. For each sample size n we consider, we estimate each posterior probability (and their order statistic) using the linear approximations on the logit scale: $\hat{p}_{n, q, \mathbf{u}_r^{(h)}}^{\delta_U - \delta_L}$ for $r = 1, \dots, m$ and $h = 0, 1$. We use Algorithm 1 to approximate $p_{n, q, \mathbf{u}_r^{(1)}}^{\delta_U - \delta_L}$ for points $\{\mathbf{u}_r^{(1)}\}_{r=1}^{m_0}$ that correspond to order statistics of $\hat{p}_{n, q, \mathbf{u}_r^{(1)}}^{\delta_U - \delta_L}$ near $\lfloor m\beta \rfloor$. If $2m\beta < m_0$, these order

statistics are the smallest m_0 ones; otherwise, we consider the order statistics ranging from $\lfloor m\beta \rfloor - m_0/2 + 1$ to $\lfloor m\beta \rfloor + m_0/2$. Similarly, we only approximate $p_{n,q,\mathbf{u}_r^{(0)}}^{\delta_U - \delta_L}$ for points $\{\mathbf{u}_r^{(0)}\}_{r=1}^m$ that correspond to order statistics of $\hat{p}_{n,q,\mathbf{u}_r^{(0)}}^{\delta_U - \delta_L}$ near $\lceil m(1-\alpha) \rceil$. If $2m\alpha < m_0$, these order statistics are the largest m_0 ones; otherwise, we consider the order statistics ranging from $\lfloor m(1-\alpha) \rfloor - m_0/2 + 1$ to $\lfloor m(1-\alpha) \rfloor + m_0/2$. When computing power and the type I error rate, we assume the $p_{n,q,\mathbf{u}_r^{(h)}}^{\delta_U - \delta_L}$ values for the remaining points do not differ enough from their estimates $\hat{p}_{n,q,\mathbf{u}_r^{(h)}}^{\delta_U - \delta_L}$ to impact the order statistics in Line 11. This approach allows us to accommodate minor discrepancies between $p_{n,q,\mathbf{u}_r^{(h)}}^{\delta_U - \delta_L}$ and $\hat{p}_{n,q,\mathbf{u}_r^{(h)}}^{\delta_U - \delta_L}$ without exploring all points $\{\mathbf{u}_r^{(0)}\}_{r=1}^m$ and $\{\mathbf{u}_r^{(1)}\}_{r=1}^m$.

Algorithm 2, however, allows us to obtain the same level of simulation precision as if we were to use all m points from each sequence to explore every sample size considered. Our method requires that we consider these $2m$ points for only three sample sizes: $n^{(0)}$, $n^{(1)}$, and $n^{(2)}$. In Lines 12 and 13, we consistently estimate power and the type I error rate at the optimal sample size $n^{(2)}$. The optimal conviction threshold is the $\lceil m(1-\alpha) \rceil^{\text{th}}$ order statistic of $p_{n^{(2)},q,\mathbf{u}_r^{(0)}}^{\delta_U - \delta_L}$. We investigate the performance and computational efficiency of this approach when considering study design for the illustrative example in Section 4.3.

4.3 Scalable Design for the Illustrative Example

We made most choices required to design a study for the illustrative example in previous sections. In Section 3.2, we specified design priors $p_D(\boldsymbol{\eta}_1)$ and $p_D(\boldsymbol{\eta}_2)$ for the conditional multinomial probabilities defined in (4) to obtain a prior $p_D(\boldsymbol{\eta}) = p_D(\boldsymbol{\eta}_1) \times p_D(\boldsymbol{\eta}_2)$ for $\boldsymbol{\eta} = (\boldsymbol{\eta}_1, \boldsymbol{\eta}_2)$. We also chose the interval $(\delta_L, \delta_U) = (-0.5, \infty)$ in Section 2 along with DIR(0.8, 0.8, 0.8, 0.8, 0.8) analysis priors for \mathbf{p}_j , $j = 1, 2$. The regions $\mathcal{G} = (-0.3, -0.1)$ and $\mathcal{R} = (-0.55, -0.5)$ were selected in Section 3.2 in recognition of the interval (δ_L, δ_U) and the anticipated effect size for the study. We define design priors for Algorithm 2 of $p_{D_1}(\boldsymbol{\eta}) \propto p_D(\boldsymbol{\eta} | \theta \sim \mathcal{U}(\mathcal{G}))$ and $p_{D_0}(\boldsymbol{\eta}) \propto p_D(\boldsymbol{\eta} | \theta \sim \mathcal{U}(\mathcal{R}))$. We described how to sample from those priors in Section 3.1. We use $m = 8192$ and $m_0 = 512$ as recommended in Section 4.2. To define operating characteristics, we choose $\alpha = 0.05$ and $\beta = 0.2$ for illustration. We consider $q = 1.25$ to reflect the reference group ($j = 2$) having roughly 25% more observations than the comparison group ($j = 1$) in Section 2. With Algorithm 2, we used the modified version of Algorithm 1 presented in Appendix C.2 of the supplement that accommodates departures from the approximate normality of $\hat{\boldsymbol{\eta}}_{1,n_1}$ and $\hat{\boldsymbol{\eta}}_{2,n_2}$.

For these inputs, Algorithm 2 returned an optimal design characterized by $(n, \gamma) = (111, 0.9341)$. For purposes of validation, we repeated this sample size calculation with a modified version of Algorithm 2 that uses binary search to explore *each* sample size n considered in a nontargeted manner with all points from the same Sobol' sequences used in the previous calculation. We obtained the *same* optimal design when exploring the sampling distributions of posterior probabilities using the nontargeted approach. We repeated the process of determining the optimal design for the illustrative example with both methods 1000 times using different Sobol' sequences $\{\mathbf{u}_r^{(1)}\}_{r=1}^m$ and $\{\mathbf{u}_r^{(0)}\}_{r=1}^m$. We obtained the exact same optimal design using

both methods in each of the 1000 repetitions.

Algorithm 2 took roughly 30 seconds with one core on a standard laptop to return an optimal design for the illustrative example. The modified version of Algorithm 2 that explored the sampling distributions of posterior probabilities in a nontargeted manner took approximately 95 seconds to obtain the same results. The discrepancy in runtime between the targeted and nontargeted approaches to explore the sampling distributions increases with the recommended sample size n . To consider a range of B consecutive sample sizes with standard binary search, we need to thoroughly explore the sampling distributions of posterior probabilities at $\mathcal{O}(\log_2 B)$ values of n . Regardless of the magnitude of the sample size recommendation, Algorithm 2 only requires that we thoroughly explore the sampling distributions at three sample sizes – the final of which is used to obtain confirmatory estimates for power and the type I error rate. In Appendix C.3 of the supplement, we also illustrate that using Sobol’ sequences instead of pseudorandom ones allows us to estimate the optimal (n, γ) combination with the same precision using three times fewer simulation repetitions.

5 Contour Plots for Design Criteria Exploration

While Algorithm 2 returns the (n, γ) combination that minimizes the sample size n while satisfying the criteria in (2) and (3), practitioners may want to explore multiple designs that are similar to the optimal one. The sampling distributions of posterior probabilities corresponding to $p_{D_1}(\boldsymbol{\eta})$ and $p_{D_0}(\boldsymbol{\eta})$ are thoroughly explored at three sample sizes in Algorithm 2: $n^{(0)}$, $n^{(1)}$, and $n^{(2)}$. These sample sizes can be ordered such that $n^{(0)} < n^{(1)} < n^{(2)}$. We approximate the sampling distributions for sample sizes less than $n^{(1)}$ using the linear approximations to $\text{logit}(p_{n,q,\mathbf{u}_r}^{\delta_U - \delta_L})$ informed by the posterior probabilities estimated at the sample sizes $n^{(0)}$ and $n^{(1)}$. For sample sizes greater than $n^{(1)}$, we use linear approximations informed by the estimated probabilities at $n^{(2)}$ instead of $n^{(0)}$. We use contour plots to synthesize these approximations to the sampling distributions. These plots visualize how changes to n and the conviction threshold γ impact power and the type I error rate.

The left column of Figure 3 illustrates the contour plots with respect to the type I error rate and power for the sample size calculation in Section 4.3. These contour plots are available with a single application of our methodology. To assist with interpretation, the green contour corresponding to power of $1 - \beta$ and the red contour corresponding to a type I error rate of α are depicted on both plots. The criteria in (2) and (3) are respectively satisfied for the regions of the (n, γ) -space that are below the green contour and above the red contour. The optimal design characterized by $(n, \gamma) = (111, 0.9341)$ is depicted by the gray point. The optimal sample size of $n = 111$ is the smallest $n \in \mathbb{Z}^+$ that is to the right of the intersection of the red and green contours.

To gain insight into how our method performs under repeated simulation, we averaged contour plots

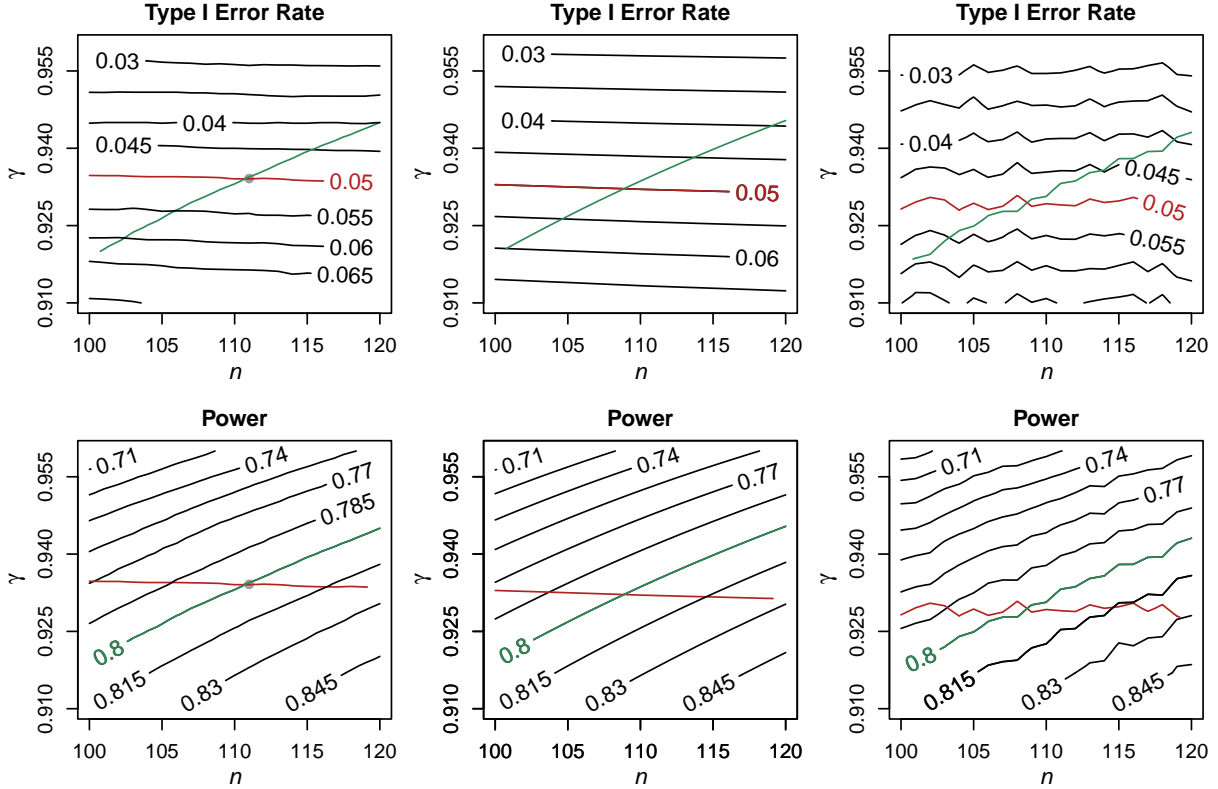


Figure 3: Left: Contour plots for the type I error rate and power for one sample size calculation with the optimal (n, γ) combination in gray. Center: Averaged contour plots from 1000 sample size calculations. Right: Contour plots estimated by simulating data.

corresponding to the 1000 repetitions of the sample size calculation from Section 4.3. These plots are given in the center column of Figure 3, but they take 1000 times as long to generate as the left plots and are not feasible to create in practice. Based on these plots, the smallest $n \in \mathbb{Z}^+$ to the right of the intersection of the green and red contours is 109. This discrepancy between $n = 111$ and 109 highlights that the optimal design differs slightly for each simulation repetition. The contour plots in the right column of Figure 3 were created by simulating $m = 81920$ samples from the prior predictive distributions for $n = \{100, 101, \dots, 120\}$ following the process detailed in Section 1. The contours in the right plots are jagged since $q = 1.25 \notin \mathbb{Z}$. The linear approximations to $\text{logit}(p_{n,q,\mathbf{u}_r}^{\delta_U - \delta_L})$ used to create the first two columns of plots in Figure 3 do not ensure that $n_2 \in \mathbb{Z}$ when $n \notin \{n^{(0)}, n^{(1)}, n^{(2)}\}$. Nevertheless, the plots in the center and right columns are similar, which is a direct consequence of Lemma 1 and the consistency of the power and type I error rate estimates at $n^{(0)}$, $n^{(1)}$, and $n^{(2)}$ via Corollary 1. The smallest $n \in \mathbb{Z}^+$ to the right of the intersection of the green and red contours in the right plots is also $n = 109$. Moreover, the fact that the center and right columns of Figure 3 do not differ much from the left column builds confidence in the single-application contour plots. In Appendix C.4 of the supplement, we illustrate why the modified version of Algorithm 1 used here yields superior performance for the illustrative example.

6 Discussion

In this paper, we developed a framework for scalable design with posterior-based operating characteristics – namely power and the type I error rate – that determines optimal sample sizes and decision criteria. The scalability of this framework stems from mapping posterior probabilities to low-dimensional hypercubes and using a targeted approach based on large-sample theory to explore the sampling distribution of posterior probabilities at most sample sizes considered. That targeted exploration approach substantially reduces the number of simulation repetitions required to design posterior analyses, making them much more attractive and accessible to practitioners that want to control type I and II error. The posterior probabilities used to determine the optimal sample size and decision criteria can also be repurposed to efficiently and helpfully investigate various sample sizes and decision criteria using contour plots.

Our proposed methods are broadly applicable and could radically reframe how data are simulated in efficient study design. They could be extended in many aspects to accommodate more complex designs. Future work could consider targeted exploration approaches that account for sequential analyses allowing for early termination or the multiple comparisons problem more generally. It may also be of interest to use these methods to design studies based on the precision of an interval estimate or maximizing the expectation of a utility function. In any of these settings, it would be pertinent to determine whether low-discrepancy sequences could be combined with targeted exploration approaches to prompt scalable design methods. This work could even be applied to make simulation-based methods more accessible in non-design settings.

Supplementary Material

These materials include a detailed description of the conditions for Theorem 1 and Lemma 1 along with their proofs and additional theoretical and simulation results. The code to conduct the numerical studies in the paper is available online: <https://github.com/lmhagar/PosteriorBasedOCs>.

Funding Acknowledgement

This work was supported by the Natural Sciences and Engineering Research Council of Canada (NSERC) by way of a PGS D scholarship as well as Grant RGPIN-2019-04212.

References

- Berry, S. M., B. P. Carlin, J. J. Lee, and P. Muller (2011). *Bayesian adaptive methods for clinical trials*. CRC press.
- Brutti, P., F. De Santis, and S. Gubbiotti (2014). Bayesian-frequentist sample size determination: a game of two priors. *Metron* 72(2), 133–151.

- Casella, G., C. P. Robert, and M. T. Wells (2004). Generalized accept-reject sampling schemes. *Lecture Notes-Monograph Series*, 342–347.
- Chaloner, K. (1996). Elicitation of prior distributions. In *Bayesian biostatistics*, pp. 141–156. Marcel Dekker, New York.
- Connor, R. J. and J. E. Mosimann (1969). Concepts of independence for proportions with a generalization of the Dirichlet distribution. *Journal of the American Statistical Association* 64(325), 194–206.
- De Santis, F. (2007). Using historical data for Bayesian sample size determination. *Journal of the Royal Statistical Society: Series A (Statistics in Society)* 170(1), 95–113.
- Elfadaly, F. G. and P. H. Garthwaite (2017). Eliciting Dirichlet and Gaussian copula prior distributions for multinomial models. *Statistics and Computing* 27(2), 449–467.
- FDA (2019). Adaptive designs for clinical trials of drugs and biologics — Guidance for industry. Center for Drug Evaluation and Research, U.S. Food and Drug Administration, Rockville, MD.
- Garthwaite, P. H., J. B. Kadane, and A. O’Hagan (2005). Statistical methods for eliciting probability distributions. *Journal of the American statistical Association* 100(470), 680–701.
- Gelman, A., J. B. Carlin, H. S. Stern, D. B. Dunson, A. Vehtari, and D. B. Rubin (2013). *Bayesian data analysis*. CRC press.
- Golchi, S. (2022). Estimating design operating characteristics in Bayesian adaptive clinical trials. *Canadian Journal of Statistics* 50(2), 417–436.
- Golchi, S. and J. Willard (2023). Estimating the sampling distribution of test-statistics in bayesian clinical trials. *arXiv preprint arXiv:2306.09151*.
- Gubbiotti, S. and F. De Santis (2011). A bayesian method for the choice of the sample size in equivalence trials. *Australian & New Zealand Journal of Statistics* 53(4), 443–460.
- Hagar, L. and N. T. Stevens (2023). Fast power curve approximation for posterior analyses. *arXiv preprint arXiv:2310.12427*.
- Jeffreys, H. (1935). Some tests of significance, treated by the theory of probability. In *Mathematical Proceedings of the Cambridge Philosophical Society*, Volume 31, No. 2, pp. 203–222. Cambridge University Press.
- Jones, G. and W. O. Johnson (2014). Prior elicitation: Interactive spreadsheet graphics with sliders can be fun, and informative. *The American Statistician* 68(1), 42–51.

- Kass, R. E. and A. E. Raftery (1995). Bayes factors. *Journal of the American Statistical Association* 90(430), 773–795.
- Lehmann, E. L. and G. Casella (1998). *Theory of point estimation*. Springer Science & Business Media.
- Lemieux, C. (2009). Using quasi–monte carlo in practice. In *Monte Carlo and Quasi-Monte Carlo Sampling*, pp. 1–46. Springer.
- Likert, R. (1932). A technique for the measurement of attitudes. *Archives of psychology* 140, 1–55.
- Morey, R. D. and J. N. Rouder (2011). Bayes factor approaches for testing interval null hypotheses. *Psychological methods* 16(4), 406–419.
- Munkhuwa, V., K. Masamba, and W. Kasapila (2022). Beta carotene apparent retention dataset, likert scale dataset, and preference ranking scale dataset. <https://doi.org/10.5281/zenodo.7180722>.
- Rubin, D. B. (1988). Using the SIR algorithm to simulate posterior distributions. *Bayesian statistics* 3, 395–402.
- Shi, H. and G. Yin (2019). Control of type I error rates in Bayesian sequential designs. *Bayesian Analysis* 14(2), 399–425.
- Smith, A. F. and A. E. Gelfand (1992). Bayesian statistics without tears: a sampling–resampling perspective. *The American Statistician* 46(2), 84–88.
- Sobol’, I. M. (1967). On the distribution of points in a cube and the approximate evaluation of integrals. *Zhurnal Vychislitel’noi Matematiki i Matematicheskoi Fiziki* 7(4), 784–802.
- Spiegelhalter, D. J., K. R. Abrams, and J. P. Myles (2004). *Bayesian approaches to clinical trials and health-care evaluation*, Volume 13. John Wiley & Sons.
- Spiegelhalter, D. J., L. S. Freedman, and M. K. Parmar (1994). Bayesian approaches to randomized trials. *Journal of the Royal Statistical Society: Series A (Statistics in Society)* 157(3), 357–387.
- Stevens, N. T. and L. Hagar (2022). Comparative probability metrics: Using posterior probabilities to account for practical equivalence in A/B tests. *The American Statistician* 76(3), 224–237.
- van der Vaart, A. W. (1998). *Asymptotic Statistics*. Cambridge Series in Statistical and Probabilistic Mathematics. Cambridge University Press.
- Wang, F. and A. E. Gelfand (2002). A simulation-based approach to bayesian sample size determination for performance under a given model and for separating models. *Statistical Science* 17(2), 193–208.

Williams, C. J., K. J. Wilson, and N. Wilson (2021). A comparison of prior elicitation aggregation using the classical method and shelf. *Journal of the Royal Statistical Society Series A: Statistics in Society* 184(3), 920–940.

Scalable Design with Posterior-Based Operating Characteristics

Supplementary Material

A Additional Content for Theorem 1

A.1 Conditions for the Bernstein-von Mises Theorem

Theorem 1 from the main text requires that the conditions for the Bernstein-von Mises (BvM) theorem are satisfied. These conditions are described in [van der Vaart \(1998\)](#), starting on page 140. Conditions (B0), (B1), and (B2) concern the likelihood component of the posterior distribution for a parameter θ . (B3) concerns the prior specifications for θ . [van der Vaart \(1998\)](#) uses θ_0 instead of θ^* to refer to the fixed parameter value, so we use that notation to state the conditions.

- (B0) The observations are drawn independently and identically from a distribution P_{θ_0} for some fixed, nonrandom θ_0 .
- (B1) The parametric statistical model from which the data are generated is differentiable in quadratic mean.
- (B2) There exists a sequence of uniformly consistent tests for testing $H_0 : \theta = \theta_0$ against $H_1 : \|\theta - \theta_0\| \geq \varepsilon$ for every $\varepsilon > 0$.
- (B3) Let the prior distribution for θ be absolutely continuous in a neighbourhood of θ_0 with continuous positive density at θ_0 .

A.2 Conditions for the Asymptotic Normality of the Maximum Likelihood Estimator

Theorem 1 from the main text also requires that the models $f(y; \boldsymbol{\eta}_1^*)$ and $f(y; \boldsymbol{\eta}_2^*)$ satisfy the regularity conditions for the asymptotic normality of the maximum likelihood estimator. These conditions should hold true for all $\boldsymbol{\eta}^* = (\boldsymbol{\eta}_1^*, \boldsymbol{\eta}_2^*)$ such that $p_D(\boldsymbol{\eta}^*) > 0$. These conditions are detailed in [Lehmann and Casella \(1998\)](#); they consider a family of probability distributions $\mathcal{P} = \{P_\theta : \theta \in \Omega\}$, where Ω is the parameter space. [Lehmann and Casella \(1998\)](#) use θ as the unknown parameter with true fixed value θ_0 , so we again state the conditions using this notation. [Lehmann and Casella \(1998\)](#) detail nine conditions that guarantee the asymptotic normality of the maximum likelihood estimator. We provide the following guidance on where to find more information about these conditions in their text. The first four conditions – (R0), (R1), (R2), and (R3) – are described on pages 443 and 444 of their text. (R4) is mentioned as part of Theorem 3.7 on

page 447. (R5), (R6), and (R7) are described in Theorem 2.6 on pages 440 and 441. (R8) is mentioned in Theorem 3.10 on page 449.

- (R0) The distributions P_θ of the observations are distinct.
- (R1) The distributions P_θ have common support.
- (R2) The observations are $\mathbf{X} = (X_1, \dots, X_n)$, where the X_i are identically and independently distributed with probability density function $f(x_i|\theta)$ with respect to a σ -finite measure μ .
- (R3) The parameter space Ω contains an open set ω of which the true parameter value θ_0 is an interior point.
- (R4) For almost all x , $f(x|\theta)$ is differentiable with respect to θ in ω , with derivative $f'(x|\theta)$.
- (R5) For every x in the set $\{x : f(x|\theta) > 0\}$, the density $f(x|\theta)$ is differentiable up to order 3 with respect to θ , and the third derivative is continuous in θ .
- (R6) The integral $\int f(x|\theta)d\mu(x)$ can be differentiated three times under the integral sign.
- (R7) The Fisher information $\mathcal{I}(\theta)$ satisfies $0 < \mathcal{I}(\theta) < \infty$.
- (R8) For any given $\theta_0 \in \Omega$, there exists a positive number c and a function $M(x)$ (both of which may depend on θ_0) such that $|\partial^3 \log f(x|\theta)/\partial \theta^3| \leq M(x)$ for all $\{x : f(x|\theta) > 0\}$, $\theta_0 - c < \theta < \theta_0 + c$, and $\mathbb{E}[M(X)] < \infty$.

A.3 Proof of Theorem 1

We prove Theorem 1 from the main text in two stages. We first prove a simpler version of Theorem 1 where the design prior $p_D(\boldsymbol{\eta})$ is degenerate (i.e., $p_D(\boldsymbol{\eta}^*) = 1$ for some $\boldsymbol{\eta}^* = (\boldsymbol{\eta}_1^*, \boldsymbol{\eta}_2^*)$ and 0 otherwise). Under the conditions for Theorem 1 in the simpler setting, the posterior mode $\tilde{\boldsymbol{\eta}}_{j,n_j}$ converges in probability to $\boldsymbol{\eta}_j^*$ for $j = 1, 2$. The following result also holds for $\mathcal{J}_j(\tilde{\boldsymbol{\eta}}_{j,n})/n_j$ in (6) from the main text:

$$\frac{1}{n_j} \mathcal{J}_j(\tilde{\boldsymbol{\eta}}_{j,n_j}) = \left[-\frac{1}{n_j} \sum_{i=1}^{n_j} \frac{\partial^2}{\partial \boldsymbol{\eta}_j^2} \log(f(y_{ij}; \boldsymbol{\eta}_j)) - \frac{1}{n_j} \frac{\partial^2}{\partial \boldsymbol{\eta}_j^2} \log(p_j(\boldsymbol{\eta}_j)) \right]_{\boldsymbol{\eta}_j = \tilde{\boldsymbol{\eta}}_{j,n_j}} \xrightarrow{P} \mathcal{I}(\boldsymbol{\eta}_j^*). \quad (\text{A.1})$$

Because $\tilde{\boldsymbol{\eta}}_{j,n_j} - \hat{\boldsymbol{\eta}}_{j,n_j} \xrightarrow{P} 0$, the mean and variance of the normal distribution in (6) from the main text respectively approximate

$$\hat{\theta}_n = g(\hat{\boldsymbol{\eta}}_{1,n_1}) - g(\hat{\boldsymbol{\eta}}_{2,n_2}) \quad \text{and} \quad \frac{1}{n} \mathcal{I}(\hat{\theta}_n)^{-1} = \sum_{j=1}^2 \frac{1}{n_j} \left[\frac{\partial g^T}{\partial \boldsymbol{\eta}} \mathcal{I}(\boldsymbol{\eta})^{-1} \frac{\partial g}{\partial \boldsymbol{\eta}} \right]_{\boldsymbol{\eta} = \hat{\boldsymbol{\eta}}_{j,n_j}},$$

for large $n = n_1 = n_2/q$ by the continuous mapping theorem. For simplicity, we do not incorporate q into the notation for $\hat{\theta}_n$ in this supplement.

It follows that when data $\mathbf{Y}^{(n,q)}$ are generated, the fraction inside the standard normal CDF of (7) from the main text converges to the following normal distribution:

$$\sqrt{n} \left(\frac{\delta - \theta^*}{\sqrt{\mathcal{I}(\hat{\theta}_n)^{-1}}} - \frac{\hat{\theta}_n - \theta^*}{\sqrt{\mathcal{I}(\hat{\theta}_n)^{-1}}} \right) \xrightarrow{d} \mathcal{N} \left(\frac{\delta - \theta^*}{\sqrt{\mathcal{I}(\theta^*)^{-1}}}, 1 \right). \quad (\text{A.2})$$

This result follows by the asymptotic normality of the MLEs $\hat{\eta}_{1,n_1}$ and $\hat{\eta}_{2,n_2}$, the continuous mapping theorem because $g(\cdot)$ is differentiable at $\boldsymbol{\eta}_1^*$ and $\boldsymbol{\eta}_2^*$, and Slutsky's theorem since $\mathcal{I}(\hat{\theta}_n)^{-1} \xrightarrow{P} \mathcal{I}(\theta^*)^{-1}$. When pseudorandom sequences $\mathbf{U} \stackrel{\text{i.i.d.}}{\sim} \mathcal{U}([0,1]^{2d})$ are input into Algorithm 1 from the main text, the maximum likelihood estimates are generated from a distribution that coincides exactly with the right side of (A.2), and the impact of the prior is negligible for large n . For the simplified case with degenerate design priors, another application of the continuous mapping theorem with the function $\Phi(\cdot)$ prompts the result $\mathcal{P}_{n,q,\mathbf{Y}^{(n,q)},(6)}^\delta \xrightarrow{d} \mathcal{P}_{n,q,\mathbf{U},Alg.1}^\delta$.

We use the previous result to prove Theorem 1 for the case with nondegenerate design priors $p_D(\boldsymbol{\eta})$. The conditions for Theorem 1 ensure that the previous result holds for all $\boldsymbol{\eta}^*$ such that $p_D(\boldsymbol{\eta}^*) > 0$. Theorem 1 assumes that $\boldsymbol{\eta}^* \sim p_D(\boldsymbol{\eta})$. For nondegenerate $p_D(\boldsymbol{\eta})$, we must integrate with respect to $\boldsymbol{\eta}$: Theorem 1 holds true by yet another application of the continuous mapping theorem. \square

B Proof of Lemma 1

B.1 Proof of Part (a)

We prove part (a) of Lemma 1 from the main text in three steps. For the first step, we prove that Algorithm 1 prompts

$$\hat{\eta}_{1,n_1,k}(\mathbf{u}_r) = \eta_{1,k}^* + \frac{\omega_k(u_1, \dots, u_k)}{\sqrt{n_1}} \quad \text{and} \quad \hat{\eta}_{2,n_2,k}(\mathbf{u}_r) = \eta_{2,k}^* + \frac{\omega_{d+k}(u_{d+1}, \dots, u_{d+k})}{\sqrt{n_2}} \quad \text{for } k = 1, \dots, d, \quad (\text{B.1})$$

where $\omega_k(\cdot)$ and $\omega_{d+k}(\cdot)$ are functions that do not depend on the sample size. In (B.1), we first consider $\mathbf{u} = (u_1, u_2, \dots, u_{2d}) \in [0,1]^{2d}$ because points of this dimension are input into Algorithm 1.

We only present the proof of (B.1) for group 1 since the proof for group 2 follows the same process. We use induction on the dimension d of $\boldsymbol{\eta}_1$ for this proof. We show the base case corresponding to a model with $d = 2$. To simplify notation, we let

$$\mathcal{I}(\boldsymbol{\eta}_1^*)^{-1} = \begin{bmatrix} \sigma_{11}^2 & \rho_{12}\sigma_{11}\sigma_{22} \\ \rho_{12}\sigma_{11}\sigma_{22} & \sigma_{22}^2 \end{bmatrix}.$$

By properties of the bivariate conditional normal distribution, it follows that

$$\hat{\eta}_{1,n_1,1}(\mathbf{u}_r) = \eta_{1,1}^* + \frac{1}{\sqrt{n_1}} \Phi^{-1}(u_1) \sigma_{11} \quad \text{and} \quad (\text{B.2})$$

$$\hat{\eta}_{1,n_1,2}(\mathbf{u}_r) = \eta_{1,2}^* + \frac{1}{\sqrt{n_1}} \sigma_{22} \left[\Phi^{-1}(u_1) \rho_{12} + \Phi^{-1}(u_2) \sqrt{1 - \rho_{12}^2} \right]. \quad (\text{B.3})$$

The result in (B.1) therefore holds true when $d = 2$, where $\omega_1(u_1)$ and $\omega_2(u_1, u_2)$ are given by the expressions to the right of the $1/\sqrt{n_1}$ terms in (B.2) and (B.3), respectively.

For the inductive hypothesis, we assume that the result in part (B.1) holds true for a model with $d = l$ parameters. For the inductive conclusion, we show that this implies the result also holds for a model with $d = l + 1$ parameters. Because $\hat{\eta}_{1,n_1,1}(\mathbf{u}_r), \dots, \hat{\eta}_{1,n_1,l}(\mathbf{u}_r)$ only depend on the components with smaller indices, we just need to prove that the result in (B.1) holds for $\hat{\eta}_{1,n_1,l+1}(\mathbf{u}_r)$. That result in conjunction with the inductive hypothesis proves the inductive conclusion. To prove the inductive conclusion, we introduce the following block matrix notation:

$$\mathcal{I}(\boldsymbol{\eta}_1^*)^{-1} = \begin{bmatrix} \boldsymbol{\Sigma}_{l,l} & \boldsymbol{\Sigma}_{l,1} \\ \boldsymbol{\Sigma}_{1,l} & \Sigma_{l+1,l+1} \end{bmatrix},$$

where $\boldsymbol{\Sigma}_{l,l}$ is a $l \times l$ matrix, $\boldsymbol{\Sigma}_{l,1}$ is a $l \times 1$ matrix, $\boldsymbol{\Sigma}_{1,l} = \boldsymbol{\Sigma}_{l,1}^T$, and $\Sigma_{l+1,l+1}$ is scalar.

The marginal distribution of $\hat{\eta}_{1,n_1,l+1}(\mathbf{u}_r)$ conditional on the already-generated $\hat{\eta}_{1,n_1,k}(\mathbf{u}_r)$ for $k = 1, \dots, l$ is

$$\mathcal{N} \left(\eta_{1,l+1}^* + \frac{1}{\sqrt{n_1}} \boldsymbol{\Sigma}_{1,l} \boldsymbol{\Sigma}_{l,l}^{-1} \begin{pmatrix} \omega_1(u_1) \\ \vdots \\ \omega_l(u_1, \dots, u_l) \end{pmatrix}, \frac{1}{n_1} \left[\Sigma_{l+1,l+1} - \boldsymbol{\Sigma}_{1,l} \boldsymbol{\Sigma}_{l,l}^{-1} \boldsymbol{\Sigma}_{l,1} \right] \right).$$

Therefore, we have that

$$\begin{aligned} \hat{\eta}_{1,n_1,l+1}(\mathbf{u}_r) &= \eta_{1,l+1}^* + \frac{1}{\sqrt{n_1}} \boldsymbol{\Sigma}_{1,l} \boldsymbol{\Sigma}_{l,l}^{-1} \begin{pmatrix} \omega_1(u_1) \\ \vdots \\ \omega_l(u_1, \dots, u_l) \end{pmatrix} \\ &\quad + \frac{1}{\sqrt{n_1}} \Phi^{-1}(u_{l+1}) \left[\Sigma_{l+1,l+1} - \boldsymbol{\Sigma}_{1,l} \boldsymbol{\Sigma}_{l,l}^{-1} \boldsymbol{\Sigma}_{l,1} \right]. \end{aligned} \quad (\text{B.4})$$

The result from (B.1) holds for $\hat{\eta}_{1,n_1,l+1}(\mathbf{u}_r)$ if we take $\omega_{l+1}(u_1, \dots, u_{l+1})$ as the sum of the two components to the right of the $1/\sqrt{n_1}$ terms in (B.4). By mathematical induction, (B.1) is true for an arbitrary model with d parameters.

The second step to prove part (a) of Lemma 1 involves showing that

$$g(\hat{\boldsymbol{\eta}}_{1,n_1}(\mathbf{u}_r)) - g(\hat{\boldsymbol{\eta}}_{2,n_2}(\mathbf{u}_r)) \approx g(\boldsymbol{\eta}_1^*) - g(\boldsymbol{\eta}_2^*) + \frac{\omega_{\dagger}(u_1, \dots, u_{2d})}{\sqrt{n}}, \quad (\text{B.5})$$

for sufficiently large $n = n_1 = n_2/q$, where $\omega_{\dagger}(\cdot)$ is a function that does not depend on n . The result in (B.5) follows from the first-order Taylor expansion of $g(\hat{\boldsymbol{\eta}}_{1,n_1}(\mathbf{u}_r)) - g(\hat{\boldsymbol{\eta}}_{2,n_2}(\mathbf{u}_r))$ around $(\boldsymbol{\eta}_1^*, \boldsymbol{\eta}_2^*)$. We have that

$$\begin{aligned} &g(\hat{\boldsymbol{\eta}}_{1,n_1}(\mathbf{u}_r)) - g(\hat{\boldsymbol{\eta}}_{2,n_2}(\mathbf{u}_r)) - (g(\boldsymbol{\eta}_1^*) - g(\boldsymbol{\eta}_2^*)) \\ &\approx \sum_{j=1}^2 \sum_{k=1}^d (-1)^{j-1} \frac{\partial g_j}{\partial \eta_{j,k}} \Big|_{(\boldsymbol{\eta}_1, \boldsymbol{\eta}_2) = (\boldsymbol{\eta}_1^*, \boldsymbol{\eta}_2^*)} [\hat{\eta}_{j,n_j,k}(\mathbf{u}_r) - \eta_{j,k}^*] \\ &\approx \frac{1}{\sqrt{n}} \left[\sum_{j=1}^2 \sum_{k=1}^d (-1)^{j-1} \frac{\partial g_j}{\partial \eta_{j,k}} \Big|_{(\boldsymbol{\eta}_1, \boldsymbol{\eta}_2) = (\boldsymbol{\eta}_1^*, \boldsymbol{\eta}_2^*)} \omega_{(j-1)d+k}(u_{(j-1)d+1}, \dots, u_{(j-1)d+k}) \right]. \end{aligned} \quad (\text{B.6})$$

The result from (B.5) follows if we let $\omega_{\dagger}(\cdot)$ be the sum on the right side of the $1/\sqrt{n}$ term in (B.6). This Taylor series expansion is suitable for large values of n – when $\hat{\eta}_{j,n_j}(\mathbf{u}_r)$ is sufficiently near $\boldsymbol{\eta}_j^*$ for $j = 1, 2$.

To prove part (a) of Lemma 1, the final step of the proof involves showing that the following result holds for sufficiently large n :

$$\begin{aligned} \frac{\delta - \underline{\theta}_r^{(n)}}{\sqrt{\underline{\mathcal{I}}_r^{(n)}}} &\approx \frac{\delta - (g(\boldsymbol{\eta}_1^*) - g(\boldsymbol{\eta}_2^*) + \omega_{\dagger}(u_1, \dots, u_{2d})/\sqrt{n})}{\sqrt{\mathcal{I}(\theta^*)^{-1}/n}} \\ &= \frac{\delta - \theta^*}{\sqrt{\mathcal{I}(\theta^*)^{-1}}} \sqrt{n} - \frac{\omega_{\dagger}(u_1, \dots, u_{2d})}{\sqrt{\mathcal{I}(\theta^*)^{-1}}}. \end{aligned} \quad (\text{B.7})$$

The approximate equivalence of the numerators in the first line of (B.7) follows from (B.5) and the fact that $\tilde{\boldsymbol{\eta}}_{j,n_j} - \hat{\boldsymbol{\eta}}_{j,n_j}$ converges in probability to 0. Moreover, $\underline{\mathcal{I}}_r^{(n)} \approx \mathcal{I}(\theta^*)^{-1}/n$ for sufficiently large n by (A.1). The second line of (B.7) holds because $\theta^* = g(\boldsymbol{\eta}_1^*) - g(\boldsymbol{\eta}_2^*)$. The expression in (B.7) takes the form $a(\delta, \theta^*)\sqrt{n} + b(\mathbf{u}_r)$ since neither fraction in the second line depends on n . Unlike (B.1), (B.5), and (B.7), part (a) of Lemma 1 considers points $\mathbf{u}_r \in [0, 1]^{2d+1}$. For a given point \mathbf{u}_r input into Algorithm 2, $\boldsymbol{\eta}^*$ is indexed by the first coordinate of \mathbf{u}_r . We clarify that the anticipated value θ^* is therefore a function of u_1 and $b(\cdot)$ is technically only a function of u_2, \dots, u_{2d+1} , where the value of each subscript can be decreased by 1 to map to the results from (B.1), (B.5), and (B.7). Part (a) of Lemma 1 follows by using the normal CDF as in (7) of the main text. We note that the function $a(\delta, \theta^*)$, which is the fraction to the left of the \sqrt{n} term in the second line of (B.7), must incorporate monotonic transformations applied to the posterior of θ to improve the suitability of its normal approximation. \square

B.2 Proof of Part (b)

To prove part (b) of Lemma 1, we introduce simplified notation, where $a(\delta_U, \theta^*) = a$ and $a(\delta_L, \theta^*) = c$. We note that $b(\mathbf{u}_r) = b$ is the same for both endpoints of the interval (δ_L, δ_U) . These simplifications yield the following result:

$$\begin{aligned} &\log(p_{n,q,\mathbf{u}_r}^{\delta_U - \delta_L}) - \log(1 - p_{n,q,\mathbf{u}_r}^{\delta_U - \delta_L}) \\ &\approx \log(\Phi(a\sqrt{n} + b) - \Phi(c\sqrt{n} + b)) - \log(1 - (\Phi(a\sqrt{n} + b) - \Phi(c\sqrt{n} + b))). \end{aligned} \quad (\text{B.8})$$

The first derivative of (B.8) with respect to n is

$$\begin{aligned} &\frac{d}{dn} [\log(\Phi(a\sqrt{n} + b) - \Phi(c\sqrt{n} + b)) - \log(1 - (\Phi(a\sqrt{n} + b) - \Phi(c\sqrt{n} + b)))] \\ &= \frac{a\phi(a\sqrt{n} + b) - c\phi(c\sqrt{n} + b)}{2\sqrt{n}(\Phi(a\sqrt{n} + b) - \Phi(c\sqrt{n} + b))} + \frac{a\phi(a\sqrt{n} + b) - c\phi(c\sqrt{n} + b)}{2\sqrt{n}(1 - (\Phi(a\sqrt{n} + b) - \Phi(c\sqrt{n} + b)))}. \end{aligned} \quad (\text{B.9})$$

We consider the limit of this derivative as $n \rightarrow \infty$ in three cases. In the first case, we consider $\theta^* \in (\delta_L, \delta_U)$. In this setting, $\Phi(a\sqrt{n} + b) - \Phi(c\sqrt{n} + b) \rightarrow 1$ as $n \rightarrow \infty$. Therefore, the limit of the first fraction in (B.9) as $n \rightarrow \infty$ is 0. The second fraction can be written in an indeterminate form, so we consider its limiting behaviour using L'Hopital's rule. We have that

$$\begin{aligned} &\lim_{n \rightarrow \infty} \frac{\frac{a}{\sqrt{n}}\phi(a\sqrt{n} + b) - \frac{c}{\sqrt{n}}\phi(c\sqrt{n} + b)}{2(1 - (\Phi(a\sqrt{n} + b) - \Phi(c\sqrt{n} + b)))} \\ &= \lim_{n \rightarrow \infty} \frac{a \left(a^2 + \frac{ab}{\sqrt{n}} + \frac{1}{n} \right) \phi(a\sqrt{n} + b) - c \left(c^2 + \frac{cb}{\sqrt{n}} + \frac{1}{n} \right) \phi(c\sqrt{n} + b)}{2(a\phi(a\sqrt{n} + b) - c\phi(c\sqrt{n} + b))}. \end{aligned} \quad (\text{B.10})$$

We must consider the limiting behaviour of (B.10) in cases. For the points in the green region where $\theta^* \in (\delta_L, \delta_U)$, $a > 0$ and $c < 0$. When $|a| < |c|$, it follows that

$$\begin{aligned}
& \lim_{n \rightarrow \infty} \frac{a \left(a^2 + \frac{ab}{\sqrt{n}} + \frac{1}{n} \right) \phi(a\sqrt{n} + b) - c \left(c^2 + \frac{cb}{\sqrt{n}} + \frac{1}{n} \right) \phi(c\sqrt{n} + b)}{2(a\phi(a\sqrt{n} + b) - c\phi(c\sqrt{n} + b))} \\
&= \lim_{n \rightarrow \infty} \frac{a \left(a^2 + \frac{ab}{\sqrt{n}} + \frac{1}{n} \right) - c \left(c^2 + \frac{cb}{\sqrt{n}} + \frac{1}{n} \right) \frac{c\phi(c\sqrt{n} + b)}{\phi(a\sqrt{n} + b)}}{2 \left(a - \frac{c\phi(c\sqrt{n} + b)}{\phi(a\sqrt{n} + b)} \right)} \tag{B.11} \\
&= \lim_{n \rightarrow \infty} \frac{a \left(a^2 + \frac{ab}{\sqrt{n}} + \frac{1}{n} \right) - c \left(c^2 + \frac{cb}{\sqrt{n}} + \frac{1}{n} \right) \exp \left(\frac{-1}{2} [(c\sqrt{n} + b)^2 - (a\sqrt{n} + b)^2] \right)}{2 \left(a - c \exp \left(\frac{-1}{2} [(c\sqrt{n} + b)^2 - (a\sqrt{n} + b)^2] \right) \right)} \\
&= \frac{a^2}{2}.
\end{aligned}$$

The last step of (B.11) follows because the limit of the exponential term in the numerator and denominator is 0 when $|a| < |c|$. When $|a| > |c|$, it follows that

$$\begin{aligned}
& \lim_{n \rightarrow \infty} \frac{a \left(a^2 + \frac{ab}{\sqrt{n}} + \frac{1}{n} \right) \phi(a\sqrt{n} + b) - c \left(c^2 + \frac{cb}{\sqrt{n}} + \frac{1}{n} \right) \phi(c\sqrt{n} + b)}{2(a\phi(a\sqrt{n} + b) - c\phi(c\sqrt{n} + b))} \\
&= \lim_{n \rightarrow \infty} \frac{a \left(a^2 + \frac{ab}{\sqrt{n}} + \frac{1}{n} \right) \exp \left(\frac{-1}{2} [(a\sqrt{n} + b)^2 - (c\sqrt{n} + b)^2] \right) - c \left(c^2 + \frac{cb}{\sqrt{n}} + \frac{1}{n} \right)}{2 \left(a \exp \left(\frac{-1}{2} [(a\sqrt{n} + b)^2 - (c\sqrt{n} + b)^2] \right) - c \right)} \tag{B.12} \\
&= \frac{c^2}{2}.
\end{aligned}$$

The last step of (B.12) follows because the limit of the exponential term in the numerator and denominator is 0 when $|a| > |c|$. When $a = -c$, the limit in (B.10) is $0.5 \times (a^3 - c^3)/(a - c) = a^2/2 = c^2/2$. Therefore, the limit of the first derivative in (B.9) is $\min\{a^2, c^2\}/2$ when $\theta^* \in (\delta_L, \delta_U)$.

In the second case for (B.9), we consider points in the red region, where a and c have the same sign. When $\theta^* > \delta_U$, $c < a < 0$, and $0 < c < a$ when $\theta^* < \delta_L$. In either case, $\Phi(a\sqrt{n} + b) - \Phi(c\sqrt{n} + b) \rightarrow 0$ as $n \rightarrow \infty$. Therefore, the limit of the second fraction in (B.9) as $n \rightarrow \infty$ is 0. The first fraction can be written in an indeterminate form, so we consider its limiting behaviour using L'Hopital's rule. We have that

$$\begin{aligned}
& \lim_{n \rightarrow \infty} \frac{\frac{a}{\sqrt{n}}\phi(a\sqrt{n} + b) - \frac{c}{\sqrt{n}}\phi(c\sqrt{n} + b)}{2(\Phi(a\sqrt{n} + b) - \Phi(c\sqrt{n} + b))} \\
&= \lim_{n \rightarrow \infty} -1 \times \frac{a \left(a^2 + \frac{ab}{\sqrt{n}} + \frac{1}{n} \right) \phi(a\sqrt{n} + b) - c \left(c^2 + \frac{cb}{\sqrt{n}} + \frac{1}{n} \right) \phi(c\sqrt{n} + b)}{2(a\phi(a\sqrt{n} + b) - c\phi(c\sqrt{n} + b))}. \tag{B.13}
\end{aligned}$$

The limit in (B.13) is just -1 times the limit in (B.10). Therefore, the limit of the first derivative in (B.9) is $-\min\{a^2, c^2\}/2$ when $\theta^* \notin [\delta_L, \delta_U]$.

The third and final case for (B.9) is when $\theta^* \in \{\delta_L, \delta_U\}$. In this scenario, we conclude that the limit of both fractions in (B.9) is 0 without appealing to L'Hopital's rule because $\Phi(a\sqrt{n} + b) - \Phi(c\sqrt{n} + b) \rightarrow 0.5$

as $n \rightarrow \infty$. Thus, the limit of (B.9) as $n \rightarrow \infty$ is 0. We emphasize that $a = 0$ if $\theta^* = \delta_U$ and $c = 0$ if $\theta^* = \delta_L$. Thus, the limit of the first derivative in (B.9) is $\min\{a^2, c^2\}/2 = 0$ when $\theta^* \in \{\delta_L, \delta_U\}$.

Putting the three cases together, we obtain part (b) of Lemma 1:

$$\begin{aligned} & \lim_{n \rightarrow \infty} \frac{d}{dn} [\log(\Phi(a\sqrt{n} + b) - \Phi(c\sqrt{n} + b)) - \log(1 - (\Phi(a\sqrt{n} + b) - \Phi(c\sqrt{n} + b)))] \\ &= \begin{cases} \frac{\min\{a^2, c^2\}}{2}, & \text{if } \theta^* \in [\delta_L, \delta_U] \\ -\frac{\min\{a^2, c^2\}}{2}, & \text{if } \theta^* \notin [\delta_L, \delta_U]. \quad \square \end{cases} \end{aligned} \quad (\text{B.14})$$

C Additional Content for the Multinomial Model

C.1 Specifying Design Priors Using the Interactive Application

To use the interface mentioned in Section 3.2 of the main text to specify $p_D(\boldsymbol{\eta}_j)$, practitioners input point estimates $\hat{p}_{j1}, \dots, \hat{p}_{jw}$ such that $\sum_{v=1}^w \hat{p}_{jv} = 1$. For the reference group ($j = 2$), we used point estimates informed by the Likert data: $(\hat{p}_{21}, \dots, \hat{p}_{25}) = (0.015, 0.015, 0.102, 0.314, 0.554)$. Initial estimates for the medians of $\{Z_{jv}\}_{v=1}^{w-1}$ are populated via (4) of the main text. Progressing from $v = 1$ to $w - 1$, practitioners consider the ξ -quantiles of each Z_{jv} variable for some $0 < \xi \neq 0.5 < 1$. These estimates for the median and ξ -quantile uniquely define marginal beta priors for each Z_{jv} variable. We used this process with $\xi = 0.95$ to specify the marginal priors for Z_{21} , Z_{22} , Z_{23} , and Z_{24} listed in Section 3.2 of the main text.

To specify $p_D(\boldsymbol{\eta}_1)$ for the comparison group, we consider the reference data and the anticipated effect size of -0.2 . The point estimates $(\hat{p}_{11}, \dots, \hat{p}_{15}) = (0.029, 0.040, 0.138, 0.305, 0.488)$ were obtained by systematically shifting probability mass to lower ordinal categories until the point estimate for the ordinal mean was 4.18. We repeated the process detailed above to specify the marginal priors for Z_{11} , Z_{12} , Z_{13} , and Z_{14} listed in Section 3.2 of the main text. A user guide with more details is available for download within the app itself.

C.2 Relaxing the Assumption on the Approximate Normality of the MLE

The posterior approximations prompted by Algorithm 1 in the main text are suitable when the sampling distributions of the MLEs $\hat{\boldsymbol{\eta}}_{1, n_1}$ and $\hat{\boldsymbol{\eta}}_{2, n_2}$ are approximately normal. The conditions for Theorem 1 guarantee that this approximate normality holds in the limiting case as $n \rightarrow \infty$. However, the quality of these normal approximations may be poor for moderate n with multinomial models where some of the individual probabilities in \boldsymbol{p} are close to 0 or 1. The illustrative example described in Section 2 of the main text is one such model: it is unlikely that children are very dissatisfied with either porridge sample as $\hat{p}_{11} = 0.0278$ and $\hat{p}_{21} = 0.0146$. Moreover, the design priors $p_{D_1}(\boldsymbol{\eta})$ and $p_{D_0}(\boldsymbol{\eta})$ assign substantial prior weight for p_{11} and p_{21} to probabilities that are even closer to 0.

The sufficient statistics for the multinomial model in group $j = 1, 2$ are $T_{j\ddagger}(\mathbf{y}^{(n, q)}) = \{T_{jv}(\mathbf{y}^{(n, q)})\}_{v=1}^w$, where $T_{jv}(\mathbf{y}^{(n, q)}) = \sum_{i=1}^{n_j} \mathbb{I}(y_{ij} = v)$. Instead of simulating $\hat{\boldsymbol{\eta}}_{1, n_1}$ and $\hat{\boldsymbol{\eta}}_{2, n_2}$ from their approximately normal

limiting distributions as in Algorithm 1, we generate approximate sufficient statistics using a continuous approximation to the binomial CDF. When $X \sim \text{BIN}(n, p^*)$, we approximate the discrete binomial variable by a continuous variable X^* such that

$$X^* \sim \begin{cases} \mathcal{U}(0, 0.5), & \text{with } Pr(X = 0) \\ \mathcal{U}(v - 0.5, v + 0.5), & \text{with } Pr(X = v) \text{ for } v = 1, \dots, n - 1 \\ \mathcal{U}(n - 0.5, n), & \text{with } Pr(X = n). \end{cases} \quad (\text{C.1})$$

It can be shown that

$$\mathbb{E}(X^*) = np^* + \frac{(1-p^*)^n - p^{*n}}{4} \quad \text{and} \quad \text{Var}(X^*) = np^*(1-p^*) + \frac{1}{12} - \frac{(1-p^*)^n(8np^* + 1) - p^{*n}(8np^* - 1)}{16}. \quad (\text{C.2})$$

From (C.2), it follows that for any $p^* \in (0, 1)$ with large n , $\mathbb{E}(X^*) \approx \mathbb{E}(X) = np^*$ and $\text{Var}(X^*) \approx \text{Var}(X) = np^*(1-p^*)$. Sufficient statistics for the multinomial model in each group *could* be obtained by iteratively sampling from (discrete) binomial distributions. However, we illustrate that such a solution would prevent us from using linear approximations to $\text{logit}(p_{n,q,\mathbf{u}_r}^{\delta_U - \delta_L})$ to explore sampling distributions of posterior probabilities in a targeted manner in Appendix C.4. Instead, we use the approach to posterior approximation presented in Algorithm 3 along with Algorithm 2 to conduct the numerical studies in Sections 4 and 5 of the main text. In Algorithm 3, we refer to X^* from (C.1) as $X^*(n, p^*)$ to emphasize the parameters of the binomial distribution being approximated.

Algorithm 3 Alternative Posterior Approximation Method for the Multinomial Distribution

- 1: **procedure** APPROXMULTINOMIAL($f(y; \boldsymbol{\eta}_1^*)$, $f(y; \boldsymbol{\eta}_2^*)$, $g(\cdot)$, n , q , \mathbf{u} , $p_1(\boldsymbol{\eta}_1)$, $p_2(\boldsymbol{\eta}_2)$)
 - 2: **for** j in $\{1, 2\}$ **do**
 - 3: **for** v in $1:w-1$ **do**
 - 4: Let $T_{jv}(\mathbf{y}^{(n,q)})$ be the $u_{(j-1)(w-1)+v}$ -quantile of $X^*(n_j - \lfloor \sum_{k=1}^{v-1} T_{jv}(\mathbf{y}^{(n,q)}) \rfloor, Z_{jv}^*)$.
 - 5: Multiply $T_{jv}(\mathbf{y}^{(n,q)})$ by $(n_j - \sum_{k=1}^{v-1} T_{jv}(\mathbf{y}^{(n,q)})) / (n_j - \lfloor \sum_{k=1}^{v-1} T_{jv}(\mathbf{y}^{(n,q)}) \rfloor)$.
 - 6: Let $T_{jw}(\mathbf{y}^{(n,q)})$ be $n_j - \sum_{k=1}^{v-1} T_{jv}(\mathbf{y}^{(n,q)})$
 - 7: Use $T_{j\ddagger}(\mathbf{y}^{(n,q)})$ to obtain the posterior mode $\tilde{\boldsymbol{\eta}}_{j,n_j}$ via optimization.
 - 8: Use $\tilde{\boldsymbol{\eta}}_{1,n_1}(\mathbf{u})$, $\tilde{\boldsymbol{\eta}}_{2,n_2}(\mathbf{u})$, $T_{1\ddagger}(\mathbf{y}^{(n,q)})$, $T_{2\ddagger}(\mathbf{y}^{(n,q)})$, and $g(\cdot)$ to obtain (7) in the main text.
-

The components of $X^*(n, p^*)$ are defined using the draw from the design prior $\boldsymbol{\eta}_j^*$. In Lines 3 to 5 of Algorithm 3, we account for having a noninteger number of observations to allocate to the remaining $w-v+1$ multinomial categories. If the remaining number of observations is noninteger, we take the ceiling of this number to be n when considering the continuous approximation to the binomial model X^* . The $\{Z_{jv}^*\}_{v=1}^{w-1}$ terms in Line 4 of Algorithm 1 are the anticipated values for the conditional multinomial probabilities in (4) of the main text. In Line 5, we apply a proportional decrease to the generated sufficient statistic to account for the noninteger number of remaining observations. While Algorithm 3 is tailored to the multinomial model, a similar process could be applied for the binomial or Poisson models if the sampling distributions of $\hat{\boldsymbol{\eta}}_{1,n_1}$ and $\hat{\boldsymbol{\eta}}_{2,n_2}$ are not approximately normal for moderate sample sizes.

We show that Algorithm 3 leads to better performance than Algorithm 1 for the illustrative example

with moderate sample sizes in Appendix C.4. Moreover, Lemma 1 still holds true when using Algorithm 3 instead of Algorithm 1. The variable X^* approximately follows a binomial distribution for large n . For sufficiently large sample sizes, the binomial distribution approximates the normal distribution. The result in (B.1) is therefore true for large sample sizes when using Algorithm 3, whereas that result holds for any $n_1, n_2 > 0$ when using Algorithm 1. The remainder of the proof of Lemma 1 in Appendix B can be applied without modifications when Algorithm 3 is used.

C.3 Benefits of Quasi-Monte Carlo Methods

We now assess the impact of using Sobol' sequences with our design procedure. In Section 4.3 of the main text, we implemented 1000 sample size calculations using Algorithm 2 for the illustrative example with Sobol' sequences of length $m = 8192$. Here, we repeated that process using Algorithm 2 with pseudorandom sequences of length $m = 8192$. We repeated that process again using pseudorandom sequences of length $m = 24000$. Given these 1000 sample size calculations, Figure C.1 depicts the density curves for the sample size recommendation n (left) and conviction threshold γ (right) corresponding to each of the three settings considered.

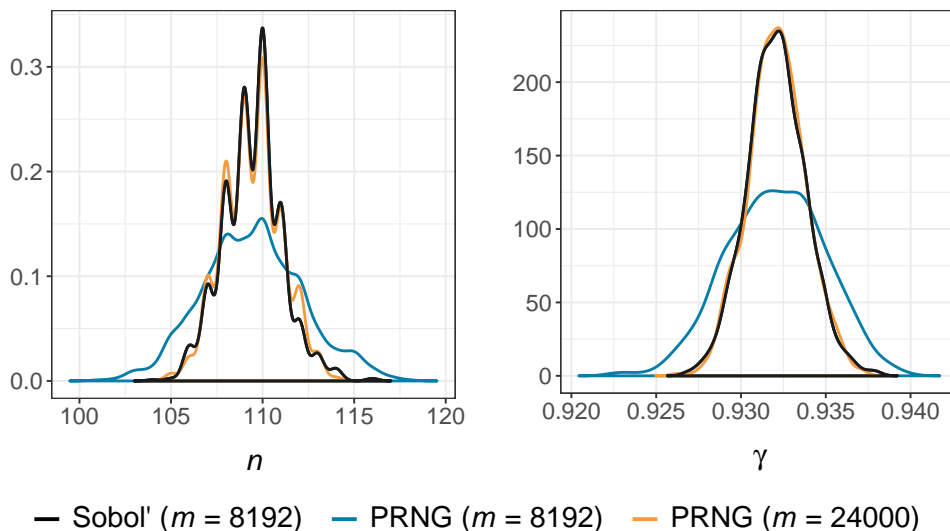


Figure C.1: Density plots of recommendations for the sample size n (left) and conviction threshold γ (right) over 1000 simulation repetitions with Sobol' and pseudorandom (PRNG) sequences of various lengths m .

Using Sobol' sequences gives rise to optimal (n, γ) recommendations that are more precise than those acquired with pseudorandom sequences. The alignment between the black and orange density curves illustrates that the (n, γ) recommendations obtained using Sobol' sequences with length $m = 8192$ are roughly as precise as those obtained with pseudorandom sequences of length $m = 24000$. For this illustrative example, Sobol' sequences therefore allow us to implement simulation-based design with the same level of precision using approximately one third of the simulation repetitions.

C.4 Illustrative Analysis Based on the Approximate Normality of the MLE

We demonstrate why using Algorithm 1 instead of Algorithm 3 with the illustrative example yields unsuitable performance. The numerical study from Section 4.3 implemented 1000 repetitions of the sample size calculation for the illustrative example using Algorithm 3. Here, we repeated this process for the same sample size calculation using Algorithm 1 instead of Algorithm 3. Following a process similar to that in Section 5 of the main text, we averaged contour plots corresponding to the 1000 repetitions of this sample size calculation. The contour plots for the type I error rate and power are given in the left column of Figure C.2. The contour plots are formatted as those in Section 5. Based on these plots, the smallest $n \in \mathbb{Z}^+$ to the right of the intersection of the green and red contours is 129. There is a substantial discrepancy between 129 and the recommendation from the averaged contour plots in Section 5 of $n = 109$. Moreover, the median recommended conviction threshold was $\gamma = 0.9440$ when using Algorithm 1 compared to $\gamma = 0.9321$ prompted by Algorithm 3.

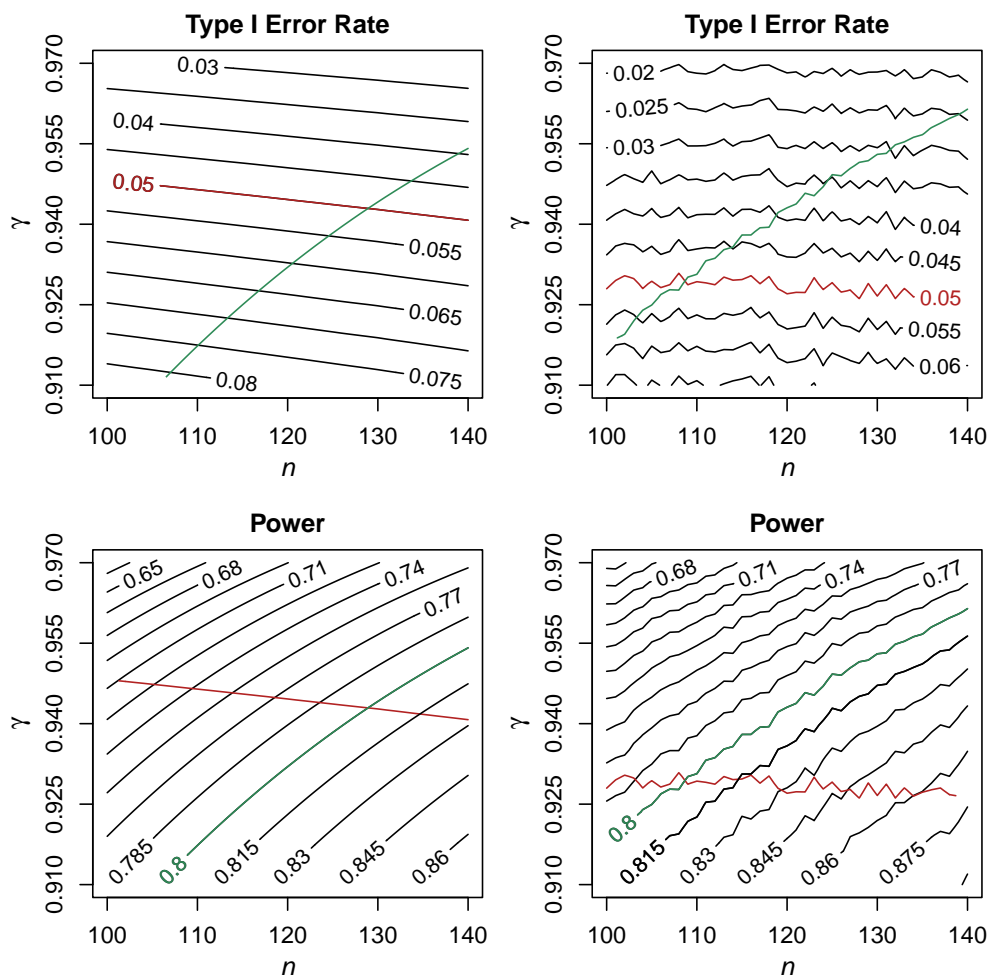


Figure C.2: Left: Averaged contour plots for the type I error rate and power from 1000 sample size calculations with Algorithm 1. Right: Contour plots estimated by simulating data.

The contour plots in the right column of Figure C.2 were created by simulating $m = 81920$ samples from the prior predictive distributions for $n = \{100, 101, \dots, 140\}$ following the process detailed in Section 1 of the main text. Again, the contours in the right plots are jagged since $q = 1.25 \notin \mathbb{Z}$. Unlike in Section 5 with Algorithm 3, the plots in the two columns are not similar when using Algorithm 1. This dissimilarity occurs because the sampling distributions for the relevant MLEs are not approximately normal for the multinomial categories with small probabilities. When implementing Algorithm 1 with the multinomial example for group $j = 1$ and 2, we generate maximum likelihood estimates for the logits of $\{Z_{jv}\}_{v=1}^{w-1}$ defined in (4) of the main text. This process ensures we do not generate maximum likelihood estimates for any components of \mathbf{p}_j that are not between 0 and 1. Figure C.3 illustrates that the sampling distribution of the MLE is not approximately normal for a sample size of $n = 109$ with a multinomial model where $Z_{11}^* = p_{11}^* = 3/108$. This anticipated value for Z_{11}^* coincides with \hat{p}_{11} : the observed proportion of children that were assigned a Likert score of 1 in the comparison group for the illustrative example in Section 2.

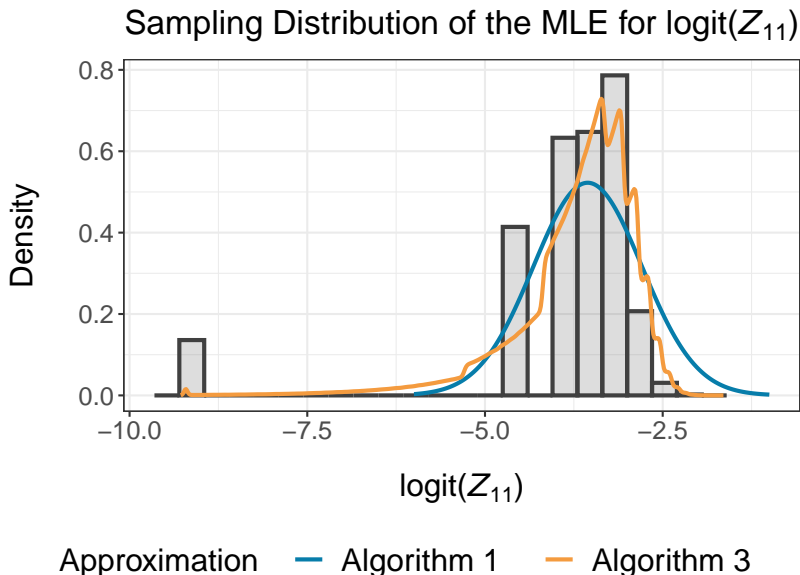


Figure C.3: Histogram of maximum likelihood estimates for the logit of Z_{11} according to the selected binomial distribution. Density curves for the approximations to this distribution prompted by Algorithms 1 (blue) and 3 (orange) are also provided.

The histogram in Figure C.3 was created by simulating 10^6 observations from the $\text{BIN}(109, 3/108)$ distribution. For each binomial sample, we took the mean of the Bernoulli observations as \hat{Z}_{11} . The histogram shows the sampling distribution of $\text{logit}(\max(\hat{Z}_{11}, 0.0001))$ to ensure that all of the maximum likelihood estimates are finite. The blue and orange density curves visualize the approximations to the sampling distribution of the MLE used by Algorithms 1 and 3, respectively. Algorithm 1 cannot accommodate the skewness of the true sampling distribution for the optimal sample size of $n = 109$, which is why Algorithm 3 yields better performance for the illustrative example. For the $\text{BIN}(n, p^*)$ model, it is standard practice to require

that $np^* > 5$ to invoke the normal approximation to the binomial distribution that Algorithm 1 relies on. For this example, nZ_{11}^* was 3.028. As such, we recommend using Algorithm 3 instead of Algorithm 1 in scenarios where $p_D(\boldsymbol{\eta}^*)$ assigns substantial prior weight to multinomial models where any of the categorical probabilities violate the $np^* > 5$ condition. It may even be advisable to consider Algorithm 3 in situations where $np^* = 5 + \epsilon$ for some small $\epsilon > 0$.

To conclude this subsection, we demonstrate why Algorithm 3 is more suitable than approaches that directly leverage discrete binomial distributions. We selected three Sobol' sequence points from the green region for the illustrative example. For each of these points $\mathbf{u}_r \in [0, 1]^{2d+1}$, we used Algorithm 3 to estimate the logit of $p_{n,q,\mathbf{u}_r}^{\delta_U - \delta_L}$ at sample sizes $n = \{90, 91, \dots, 150\}$ for the illustrative example. We then modified this process to estimate the logits of $p_{n,q,\mathbf{u}_r}^{\delta_U - \delta_L}$ by generating sufficient statistics using CDF inversion on their exact binomial distributions with the same three points from the Sobol' sequence. Figure C.4 visualizes the logit of $p_{n,q,\mathbf{u}_r}^{\delta_U - \delta_L}$ as a function of n for both types of approximations, where the functions approximated using the discrete binomial distributions are given by the solid curves. The functions approximated via Algorithm 3 are depicted using the dotted curves, and the results for each Sobol' sequence point are grouped by colour.

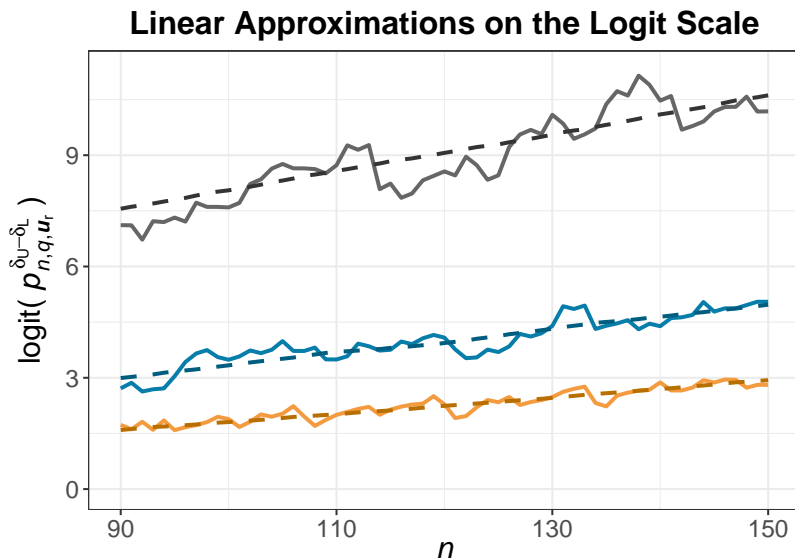


Figure C.4: The logits of $p_{n,q,\mathbf{u}_r}^{\delta_U - \delta_L}$ as a function of n for three Sobol' sequence points from the green region for the illustrative example. The curves were created using the discrete binomial model (solid) and Algorithm 3 (dotted).

We can generate sufficient statistics for the multinomial model using their exact binomial distributions; however, that process prevents the logit of $p_{n,q,\mathbf{u}_r}^{\delta_U - \delta_L}$ from being a smooth function for moderate n as a result of the binomial distribution's discreteness. It is therefore problematic to use the linear approximations to those functions to implement targeted exploration of sampling distributions of posterior probabilities. Algorithm 3 and Algorithm 1 have linear approximations to the logit of $p_{n,q,\mathbf{u}_r}^{\delta_U - \delta_L}$ that are of better quality. Since Algorithm 3 yields suitable performance as illustrated in Section 5 of the main text, we recommend that method over

ones that involve discrete distributions.

D Additional Content for Non-Exponential Family Models

D.1 Alternative Method for Posterior Approximation

Algorithm 1 from the main text must be adapted when the selected model is not a member of the exponential family. We therefore extend a hybrid approach to analytical posterior approximation from [Hagar and Stevens \(2023\)](#) that accounts for the priors when low-dimensional sufficient statistics cannot be recovered from the maximum likelihood estimates $\hat{\boldsymbol{\eta}}_{1,n_1}$ and $\hat{\boldsymbol{\eta}}_{2,n_2}$. That hybrid approach leverages the following result, which holds true when $\boldsymbol{\eta}_j \approx \hat{\boldsymbol{\eta}}_{j,n_j}$ for sufficiently large n_j :

$$\log(p_j(\boldsymbol{\eta}_j | \mathbf{y}^{(n)})) \approx l(\hat{\boldsymbol{\eta}}_{j,n_j}; \mathbf{y}^{(n,q)}) - \frac{n_j}{2} (\boldsymbol{\eta}_j - \hat{\boldsymbol{\eta}}_{j,n_j})^T \mathcal{I}(\hat{\boldsymbol{\eta}}_{j,n_j}) (\boldsymbol{\eta}_j - \hat{\boldsymbol{\eta}}_{j,n_j}) + \log(p_j(\boldsymbol{\eta}_j)). \quad (\text{D.1})$$

This result follows from the second-order Taylor approximation to the log-posterior of $\boldsymbol{\eta}_j$ around $\hat{\boldsymbol{\eta}}_{j,n_j}$, where the observed information is replaced with the (expected) Fisher information. Although the first term on the right side of (D.1) depends on the data $\mathbf{y}^{(n,q)}$, it is a constant. An approximation to the posterior mode is the value that maximizes the right side of (D.1): $\check{\boldsymbol{\eta}}_{j,n_j}$.

We consider the following normal approximation to the posterior of θ :

$$\mathcal{N} \left(g(\check{\boldsymbol{\eta}}_{1,n_1}) - g(\check{\boldsymbol{\eta}}_{2,n_2}), \sum_{j=1}^2 \left[\frac{\partial g^T}{\partial \boldsymbol{\eta}} \check{\mathcal{J}}_j(\boldsymbol{\eta})^{-1} \frac{\partial g}{\partial \boldsymbol{\eta}} \right]_{\boldsymbol{\eta}=\check{\boldsymbol{\eta}}_{j,n_j}} \right), \quad \text{where } \check{\mathcal{J}}_j(\boldsymbol{\eta}) = n_j \mathcal{I}(\boldsymbol{\eta}) - \frac{\partial^2}{\partial \boldsymbol{\eta}^2} \log(p_j(\boldsymbol{\eta})). \quad (\text{D.2})$$

The observed information is again replaced with the Fisher information in $\check{\mathcal{J}}_j(\boldsymbol{\eta})$ of (D.2) since we do not generate samples $\mathbf{y}^{(n,q)}$. Algorithm 4 details how we can obtain the posterior approximation in (D.2) using a single point $\mathbf{u} \in [0, 1]^{2d}$.

Algorithm 4 Low-Dimensional Posterior Approximation with Hybrid Method

- 1: **procedure** APPROXHYBRID($f(y; \boldsymbol{\eta}_1^*)$, $f(y; \boldsymbol{\eta}_2^*)$, $g(\cdot)$, n , q , \mathbf{u} , $p_1(\boldsymbol{\eta}_1)$, $p_2(\boldsymbol{\eta}_2)$)
 - 2: Generate $\hat{\boldsymbol{\eta}}_{1,n_1}(\mathbf{u})$ and $\hat{\boldsymbol{\eta}}_{2,n_2}(\mathbf{u})$ using Lines 2 to 4 of Algorithm 1 from the main text.
 - 3: **for** j in $\{1, 2\}$ **do**
 - 4: Obtain $\check{\boldsymbol{\eta}}_{j,n_j}$ as $\arg \max_{\boldsymbol{\eta}_j}$ of the right side of (D.1) when $\boldsymbol{\eta}_{j,n_j} = \hat{\boldsymbol{\eta}}_{j,n_j}(\mathbf{u})$.
 - 5: Use $\check{\boldsymbol{\eta}}_{1,n_1}$, $\check{\boldsymbol{\eta}}_{2,n_2}$, and the partial derivatives of $g(\cdot)$ to obtain (D.2).
-

The results from Theorem 1 and Lemma 1 hold true when using Algorithm 4 instead of Algorithm 1. The result in Theorem 1 is straightforward because $\check{\boldsymbol{\eta}}_{j,n_j} - \hat{\boldsymbol{\eta}}_{j,n_j}$ converges in probability to 0, and $\check{\mathcal{J}}_j(\check{\boldsymbol{\eta}}_{j,n_j})/n_j$ converges in probability to $\mathcal{I}(\boldsymbol{\eta}_j^*)$ following similar logic to (A.1). To prove the result in part (a) of Lemma 1, we argue that $\underline{\tau}_r^{(n)} \approx \mathcal{I}(\theta^*)^{-1}/n$ for sufficiently large n once again by similar logic to (A.1) when Algorithm 4 is used. No modifications to Appendix B.2 are required to prove part (b) of Lemma 1.

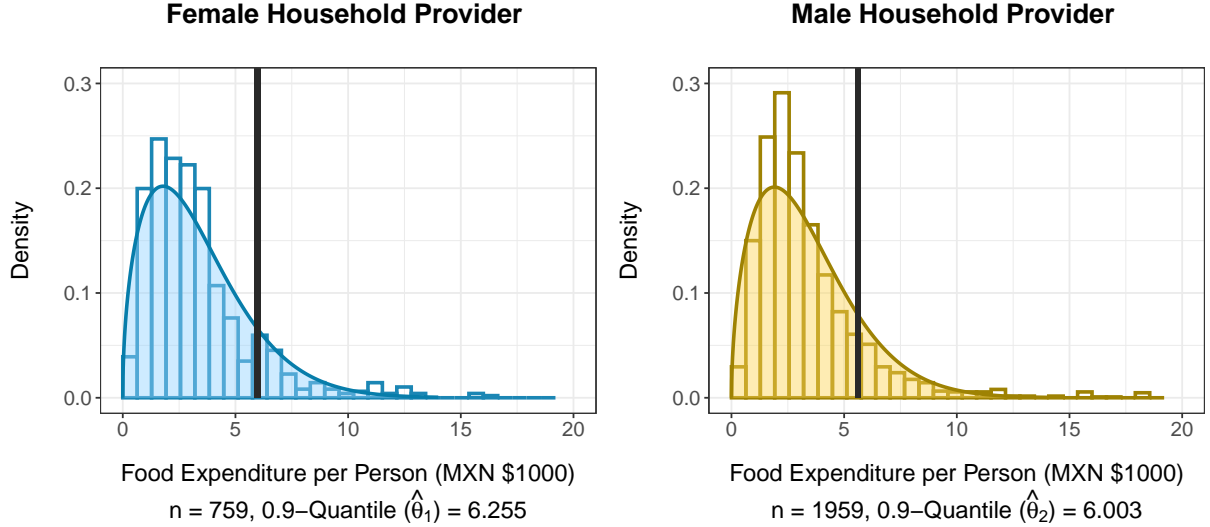


Figure D.1: Distribution of quarterly food expenditure per person in each group.

D.2 Illustrative Analysis with the Weibull Model

Mexico’s National Institute of Statistics and Geography conducts a biennial survey to monitor household income and expenses along with sociodemographic characteristics. We refer to this survey by its Spanish acronym ENIGH. In the ENIGH 2020 survey (INEGI, 2021), each surveyed household was assigned a socioeconomic class. We use data from lower-middle income households (the most populous class) in the Mexican state of Aguascalientes. We split the households into two groups based on the sex of the household’s main provider. Each household has a weighting factor used to include its observation between one and four times in our data set. The datum y_{ij} collected for each household $i = 1, \dots, n_j$, $j = 1, 2$ is its quarterly expenditure on food per person measured in thousands of Mexican pesos (MXN \$1000). We exclude the 0.41% of households that report zero quarterly expenditure on food to accommodate the Weibull model’s positive support. This respectively yields $n_1 = 759$ and $n_2 = 1959$ observations in the female ($j = 1$) and male ($j = 2$) provider groups that are visualized in Figure D.1.

We compare the 0.9-quantile for each distribution; that is, $\theta_j = F_j^{-1}(0.9)$, where $F_j(\cdot)$ is the cumulative distribution function for distribution $j = 1, 2$. We use the ratio θ_1/θ_2 to consider whether the 0.9-quantiles of food expenditure in the female and male provider groups are practically equivalent. The observed 0.9-quantiles of quarterly food expenditure per person (in MXN \$1000) are $\hat{\theta}_1 = 6.255$ and $\hat{\theta}_2 = 6.003$. We assign uninformative GAMMA(2, 1) priors to both the shape ν_j and rate λ_j parameters of the Weibull model for group $j = 1, 2$. We let $\boldsymbol{\eta}_j = (\nu_j, \lambda_j)$ for $j = 1, 2$. We obtain 10^5 posterior draws for $\boldsymbol{\eta}_1$ and $\boldsymbol{\eta}_2$ using Markov chain Monte Carlo (MCMC). The Weibull distributions characterized by the posterior means for $\boldsymbol{\eta}_1$ and $\boldsymbol{\eta}_2$ are superimposed on the histograms in Figure D.1. Since the Weibull distribution is a reasonable model for these data, we use this example to illustrate our extensions for non-exponential models in this section.

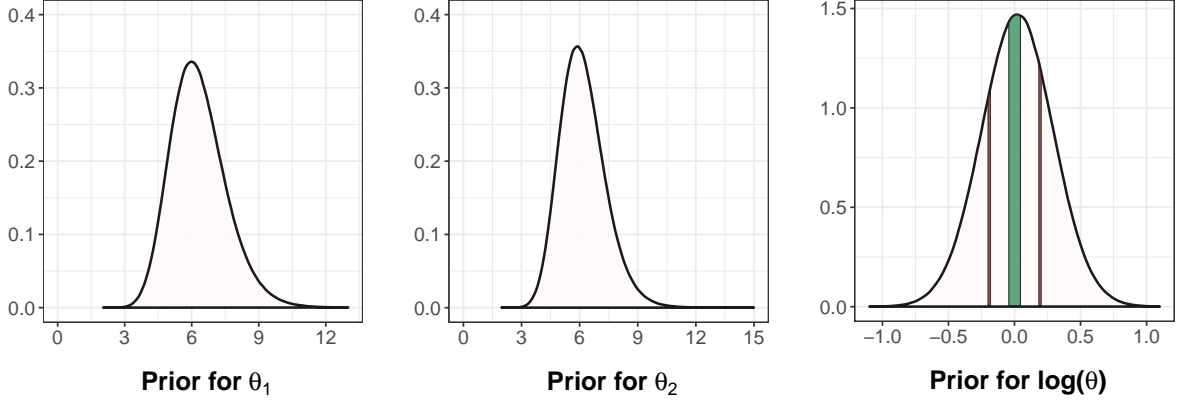


Figure D.2: Induced design priors for θ_1 (left), θ_2 (centre), and $\log(\theta)$ (right). The green and red regions of the θ -space are visualized on the logarithmic scale on the right plot.

We next choose design and analysis priors for this example. Because the ENIGH survey is conducted biennially, we choose design priors for η_1 and η_2 using data from the ENIGH 2018 survey (INEGI, 2019). We repeated the process described above to create a similar data set of 2018 quarterly food expenditure per person. We adjusted each expenditure to account for inflation, compounding 2% annually, between 2018 and 2020. For group j , we obtained posteriors for ν_j and λ_j given these data and GAMMA(2,1) priors for each parameter. To define priors, we consider gamma distributions that have the same modes with variances that are larger by factors of 30 and 100 for groups 1 and 2, respectively. These distributions are GAMMA(38.07, 26.23) for ν_1 , GAMMA(34.92, 10.02) for λ_1 , GAMMA(38.35, 25.09) for ν_2 , and GAMMA(37.51, 10.70) for λ_2 .

We use those gamma distributions to obtain the design priors $p_{D_1}(\eta)$ and $p_{D_0}(\eta)$ for this example. Figure D.2 visualizes the priors for θ_1 , θ_2 , and $\log(\theta) = \log(\theta_1) - \log(\theta_2)$ that are induced by those gamma distributions. For illustration, we choose the interval (δ_L, δ_U) to be $(1.2^{-1}, 1.2)$. This choice indicates that a 20% relative increase or decrease in the 0.9-quantile is not of practical importance. We define the regions \mathcal{G} and \mathcal{R} based on the general guidance from Section 3.2 of the main text. The region $\mathcal{G} = (1.05^{-1}, 1.05)$ is centred around exact equivalence of 1 on the relative scale. For this example, $\mathcal{R} = (1.225^{-1}, 1.2^{-1}) \cup (1.2, 1.225)$ is contiguous with both endpoints of the interval (δ_L, δ_U) , where each interval in this union is narrow. These red and green regions are depicted on the logarithmic scale in the right plot of Figure D.2. We now define design priors of $p_{D_1}(\eta) \propto p_D(\eta | \log(\theta) \sim \mathcal{U}(\log(\mathcal{G})))$ and $p_{D_0}(\eta) \propto p_D(\eta | \log(\theta) \sim \mathcal{U}(\log(\mathcal{R})))$, where $p_D(\eta)$ is created by independently joining the gamma priors from the previous paragraph. Here, the conditioning used to define these priors ensures that θ is uniformly distributed over the red and green regions on the logarithmic scale. We independently join marginal GAMMA(2, 0.1) priors for ν_j and λ_j to obtain an analysis prior $p_j(\eta_j)$ for group $j = 1, 2$. Our final inputs for Algorithm 2 are $m = 8192$, $m_0 = 512$, $\alpha = 0.1$, $\beta = 0.3$, $q = 1$.

When using Algorithm 4 to implement posterior approximation, Algorithm 2 returned an optimal design characterized by $(n, \gamma) = (163, 0.8795)$. As in Section 4.3 of the main text, we repeated this sample size calculation 1000 times with different Sobol' sequences $\{\mathbf{u}_r^{(1)}\}_{r=1}^m$ and $\{\mathbf{u}_r^{(0)}\}_{r=1}^m$. For each repetition, the optimal design coincided with the (n, γ) recommendation obtained by exploring the sampling distributions of posterior probabilities with nontargeted approaches using the same Sobol' sequences. For this Weibull example, Algorithm 2 took roughly 25 seconds on a standard laptop without parallelization to return an optimal design for the illustrative example. The modified version of Algorithm 2 that explored the sampling distributions of posterior probabilities in a nontargeted manner took approximately 90 seconds. Using the process described in Section 5 of the main text, we averaged contour plots for the type I error rate and power corresponding to the 1000 repetitions of the sample size calculation for the Weibull example. These plots are given in the left column of Figure D.3. Based on these plots, the smallest $n \in \mathbb{Z}^+$ to the right of the intersection of the green and red contours is 162.

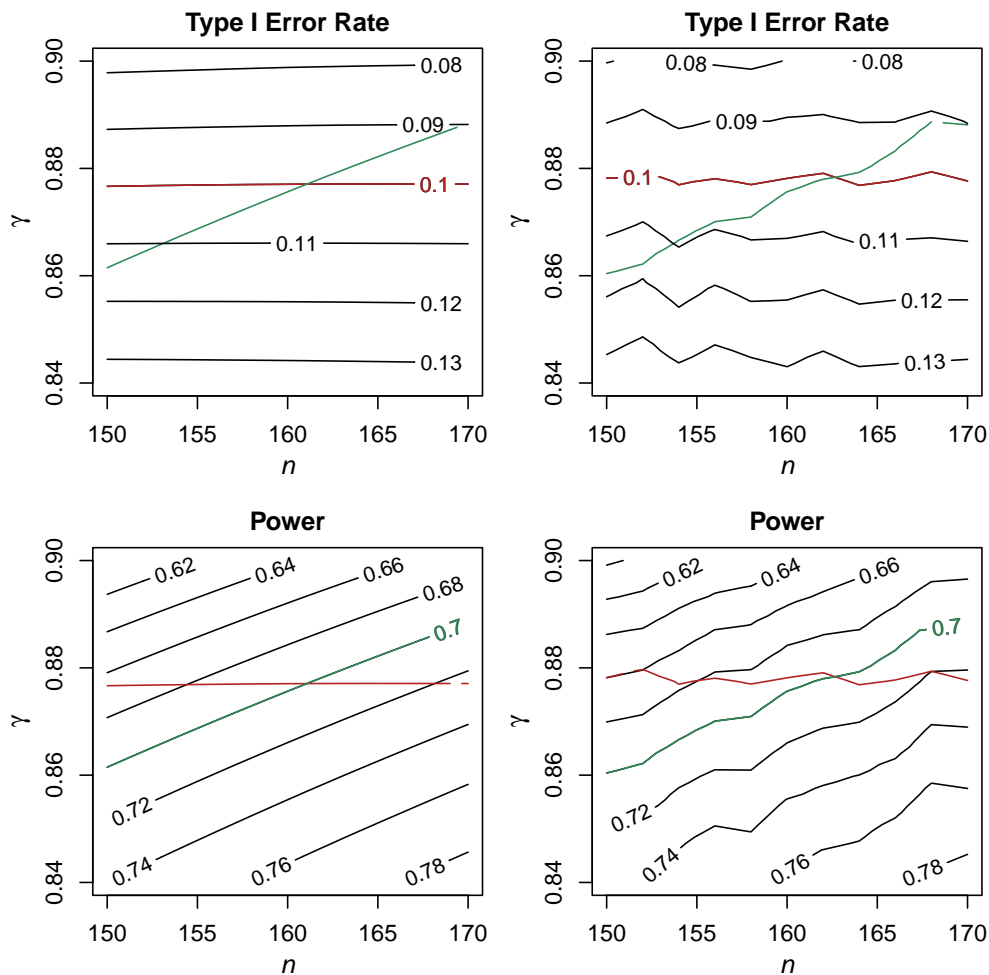


Figure D.3: Left: Averaged contour plots for the type I error rate and power from 1000 sample size calculations with Algorithm 4 and the Weibull example. Right: Contour plots estimated by simulating data.

The contour plots in the right column of Figure D.3 were created by simulating $m = 40960$ samples from the prior predictive distributions for $n = \{150, 152, \dots, 170\}$ following the process detailed in Section 1. The contours in the right plots are less jagged than those for the multinomial example since $q = 1$. However, the contours in the right column are still more jagged than those in the left column because the left plots consider the sampling distributions of posterior probabilities with the same points $\{\mathbf{u}_r^{(1)}\}_{r=1}^m$ and $\{\mathbf{u}_r^{(0)}\}_{r=1}^m$ for *each* sample size. The sampling distributions of posterior probabilities in the right plots are estimated independently for each value of n considered. The smallest $n \in \mathbb{Z}^+$ to the right of the intersection of the green and red contours in the right plots is $n = 163$. The plots in the left and right columns are similar, which illustrates that using Algorithm 4 to approximate posteriors for this non-exponential family example prompts suitable performance.

References

- Hagar, L. and N. T. Stevens (2023). Fast power curve approximation for posterior analyses. *arXiv preprint arXiv:2310.12427*.
- Instituto Nacional de Estadística, Geografía e Informática [National Institute of Statistics, Geography, and Informatics] (INEGI) (2019). Encuesta Nacional de Ingresos y Gastos de los Hogares (ENIGH). 2018 Nueva serie [National Survey of Household Income and Expenses. New edition 2018]. www.inegi.org.mx/programas/enigh/nc/2018/#Datos_abiertos.
- Instituto Nacional de Estadística, Geografía e Informática [National Institute of Statistics, Geography, and Informatics] (INEGI) (2021). Encuesta Nacional de Ingresos y Gastos de los Hogares (ENIGH). 2020 Nueva serie [National Survey of Household Income and Expenses. New edition 2020]. www.inegi.org.mx/programas/enigh/nc/2020/#Datos_abiertos.
- Lehmann, E. L. and G. Casella (1998). *Theory of Point Estimation*. Springer Science & Business Media.
- van der Vaart, A. W. (1998). *Asymptotic Statistics*. Cambridge Series in Statistical and Probabilistic Mathematics. Cambridge University Press.